João Pedro Fernandes Andrade

Licenciatura Biologia

Pleistocene biostratigraphic markers of the North Pacific, IODP Site U1340: *Proboscia barboi*, *Proboscia curvirostris* and *Thalassiosira jouseae*

Dissertação para obtenção do Grau de Mestre em Paleontologia

FACULDADE DE CIÊNCIAS E TECNOLOGIA
UNIVERSIDADE NOVA DE LISBOA

Março, 2016

João Pedro Fernandes Andrade

Licenciatura Biologia

Pleistocene biostratigraphic markers of the North Pacific, IODP Site U1340: *Proboscia barboi*, *Proboscia curvirostris* and *Thalassiosira jouseae*

Dissertação para obtenção do Grau de Mestre em Paleontologia

Orientadora: Zuzanna Stroynowski, Investigadora, IPMA
Co-orientador: Paulo Legoinha, Professor auxiliar, FCT

Júri:

Presidente: Fernando Reboredo
Arguente: Fátima Abrantes
Vogal: Zuzanna Stroynowski

FACULDADE DE CIÊNCIAS E TECNOLOGIA
UNIVERSIDADE NOVA DE LISBOA

Março, 2016

Foreword and acknowledgements

The original aim of this thesis was to study Miocene diatoms from the Belverde Borehole (Península de Setúbal) in order to: 1) establish a diatom-based biostratigraphy and complement the well-established biostratigraphy based on foraminifera and nannoplankton (Legoinha and Flores, 2014), and 2) characterize diatom paleoecological associations and thereby better understand the paleogeographic and paleoenvironmental evolution of the Lower Tagus Basin and complement previous studies based on other microfossil groups. Unfortunately, the Belverde Borehole proved to be barren of any siliceous microfossils and only one outcrop sample yielded diatom frustules. Therefore the subject had to be reformulated, having my advisor Dr. Zuzia Stroynowski conveniently suggested the study of Plio-Pleistocene diatom species at IODP Site U1340 in the Bering Sea. The study of the Belverde Borehole diatoms is presented in the Annex.

I should express my gratitude to my advisor Dr. Zuzia Stroynowski, for the help and counseling throughout the process of accomplishing this dissertation, my co-advisor Dr. Paulo Legoinha for his assistance and accessibility, Dr. Fátima Abrantes, who gave me the opportunity to work on my master's degree dissertation at the Instituto Português do Mar e da Atmosfera (IPMA) by indication of Dr. Paulo Legoinha, and Dr. Brian Ottway for helping identify the diatoms from the Belverde Borehole study. I am also thankful to my colleagues at IPMA who were always willing to help and support me.

Lastly, I thank my family and friends for their kind support.

Abstract

Diatoms are a large and widespread group of phytoplankton with an important role in ecosystems as primary producers. They are of great use in biostratigraphic and paleoclimatic studies, namely in the Bering Sea, where they are abundantly preserved in sediments. *Proboscia barboi*, *Proboscia curvirostris* and *Thalassiosira jouseae* are Plio-Pleistocene centric diatoms of mid to high latitudes of the North Pacific and North Atlantic Oceans, and are important biostratigraphic markers and datums in these regions. In this study, the biostratigraphy of these species at IODP Site U1340 (Bowers Ridge, Bering Sea) is refined and their abundance record interpreted in light of the paleoclimatic context of the North Pacific during the Plio-Pleistocene, using environmental information from the diatom assemblage in order to better understand the ecology of these extinct species. On a morphological approach, *T. jouseae* and its close related species *Thalassiosira nidulus* are described based on specimens of Site U1340 and their differences discussed. In addition, evidence for the evolutionary link between *P. barboi* and *P. curvirostris* is provided and discussed.

Keywords: diatoms, Bering Sea, Site U1340, *Proboscia curvirostris*, *Proboscia barboi*, *Thalassiosira jouseae*

Resumo

As diatomáceas são um grande grupo de fitoplâncton com uma distribuição global, que desempenha um papel importante nos ecossistemas como produtores primários. Têm uma aplicação fundamental em estudos de biostratigrafia e paleoclimatologia, nomeadamente no Mar de Bering, onde se encontram abundantemente preservados nos sedimentos. *Proboscia barboi*, *Proboscia curvirostris* e *Thalassiosira jouseae* são diatomáceas cêntricas de latitudes média-altas do Pacífico Norte e Atlântico Norte, e importantes marcadores e datums biostratigráficos nestas regiões. Neste estudo, a biostratigrafia destas espécies na sondagem do IODP U1340A (Bowers Ridge, Mar de Bering) é refinada e o seu registo de abundância interpretado no contexto paleoclimático do Pacífico Norte durante o Plio-Plistocénico e recorrendo a espécies de diatomáceas indicadoras de ambiente, de maneira a estudar sua ecologia. De uma perspectiva morfológica, *T. jouseae* e uma espécie taxonomicamente próxima *Thalassiosira nidulus*, são descritas com base em exemplares da sondagem U1340A e as suas diferenças discutidas. Adicionalmente, a relação evolutiva entre *P. barboi* e *P. curvirostris* é evidenciada.

Termos chave: diatomáceas, Mar de Bering, Sondagem U1340A, *Proboscia curvirostris*, *Proboscia barboi*, *Thalassiosira jouseae*

List of Contents

List of Figures

List of Tables

Acronyms

APC – Advanced piston corer

AS – Alaskan Stream

BSC – Bering Slope Current

DSDP – Deep Sea Drilling Project

DSF – Drilling depth below seafloor

FCO – First common occurrence

FO – First occurrence

FOV – Fields of view

IODP – International Ocean Drilling Project

LM – Light microscope

LCO – Last common occurrence

LO – Last occurrence

MFSF – Mat-forming shade flora species

MPT – Mid-Pleistocene Transition

NHG – Northern Hemisphere Glaciation

NPD – North Pacific Diatom (zonation/zone)

RA – Relative abundance

XCB – Extended core barrel

1 Introduction

1.1 Diatoms

Diatoms are a large group of unicellular phototrophic algae with sizes ranging from 10 to 200 µm, which inhabit a wide range of aquatic and semi-aquatic environments. The most distinguishing feature of diatoms is the silica shell or exoskeleton - frustule - which consist of a highly differentiated cell wall heavily impregnated with silica. The frustule is characterized for its diverse shapes and ornamentations and has been since the first microscopic observations in the XVIII century, the main source of taxonomic characters. Diatoms often establish colonies by a variety of means e.g. producing mucus threads, and thereby forming chains of several millimetres.

Being photosynthetic microorganisms, diatoms are restricted to aquatic and semi-aquatic environments with sufficient light exposure. They commonly live as part of the phytoplankton community in the surface water (down to 200 m) or have a benthic lifestyle, and as such have an important role in ecosystems as primary producers. In fact, they are the dominant marine primary producers, being responsible for 40-45% of ocean's primary production (Mann, 1999). Also, production of biogenic silica in the ocean is mainly attributed to diatoms which therefore play an important role in the ocean's silica cycle, in addition to the carbon cycle (Tréguer and De La Rocha, 2013). In coastal, equatorial and high latitude upwelling regions, diatoms dominate the phytoplankton communities and typically exhibit bloom-and-bust cycles where their numbers exponentially increase when nutrients and light become available, and upon depletion of nutrients (e.g. Si), sinking rates increase, spores may form and eventually fall to the sediment. In some cases in the past, such massive quantities of diatoms were deposited on the sea floor that through diagenetic processes, the deposits turned into diatomite, a rock entirely formed of frustules that today is of great commercial interest. Thus diatoms play a key role as producers and regulators of the ocean's both silica and carbon cycles.

Diatoms belong to Division Chrysophyta, class Bacillariophyceae and are organized in two orders based on symmetry (Abrantes and Gil, 2007):

- Pennales; pennate diatoms
- Centrales; centric diatoms

Pennate diatoms have bilateral symmetry and mostly live in freshwater, soil or attached to a substrate (e.g. sand grains, plants). Many pennate diatoms bear an unsilicified groove along the apical axis of the valve, called the raphe, which is involved in the secretion of mucus that aids locomotion. The raphe is exclusive to pennate diatoms. Centric diatoms have radial symmetry and often live in marine waters as phytoplankton.

The oldest diatom fossils date back to the Early Jurassic and consist of centric forms, while pennate diatoms are a more recent group, only appearing in the Late Cretaceous from a radiation of centric diatoms. However, genomic studies suggest an earlier origin for diatoms, during the Mesozoic (Armstrong and Brasier, 2013; Sims et al., 2006).

1.2 The frustule

The frustule is the silica exoskeleton of the diatom cell and during its lifetime, is covered by a thin organic coat. Although characterized for its diverse morphology, the frustule has a basic composition, organization and morphologic features common to all diatoms.

The frustule is a multipartite structure composed of two valves, the epivalve and the hypovalve, which are connected by a series of thinner linking structures called the girdle elements. These surround the region in between the two valves and are collectively named girdle or cincture. The girdle elements associated with the epivalve are termed epicingulum, which together with the epivalve form the epitheca, while the hypovalve together with the hypocingulum forms the hypotheca. The organization of the frustule resembles the two halves of a petri-dish in the sense that the hypotheca underlies the edge of the epitheca (fig. 1.1). All components of the frustule fit together very closely and enclose the cytoplasm, allowing communication with the exterior, mainly via pores and slits in the wall components.

The frustule may be observed in two main orientations: the valve view, where the valve face is fully visible and the girdle view, when the frustule is visualized in profile. The diatom cell often has different outlines depending on the orientation. The valve view generally provides more features for identification and therefore is preferred for identification of diatom specimens. Pennate diatoms have an elliptical or rectangular outline in valve view, while centric diatoms are generally circular, triangular or quadrate in valve view, and rectangular or ovate in girdle view (Armstrong and Brasier, 2013; Round et al., 1990).

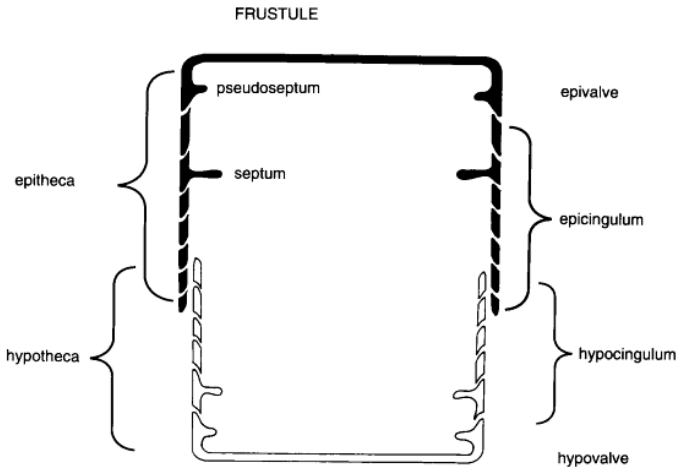

Figure 1.1 - Gross morphology of the frustule in cross section view. (Hasle et al., 1996).

The valve is regularly perforated by areolae or pores, whose arrangement forms a pattern (i.e. areolation) which is an important taxonomic feature. Rows of areolae form striae and the non-perforated areas of the valve surface between striae are called interstriae or costae. The valve mantle is the marginal area or edge of the valve (Round et al., 1990).

1.3 Reproduction

Diatoms reproduce vegetatively by binary fission, forming two individuals within the frustule of the parent cell. As a consequence of this type of cell division, with the formation of new siliceous components inside the parent cell, the cell size of each generation progressively diminishes. Maximal cell size is restored by auxospore formation, a process usually linked to sexual reproduction. It is also a size dependent process which usually occurs when a cell reaches about a third of its maximal size and cannot take place below this threshold. Small cells unable to develop auxospores keep dividing until division is no longer viable. This in turn, means that certain species are not found beyond a certain size range, and again, are a diagnostic feature used in taxonomic identification.

Diatoms are diplont algae. While centric diatoms are usually oogamous with flagellated male gametes, most pennate diatoms are isogamous and lack a flagellated stage. The development of the auxospore begins right after plasmogamy between the two gametes when the cell is at a binuclear stage, which may be transient or last many hours until the nuclei have fused. The first step is the formation of an organic wall which in some centric genera may bear siliceous scales. The auxospore then expands; a process that may be more or less isometrical, depending on the symmetry of the cell. In centric taxa with simple radial symmetry the

expansion is nearly spherical whereas in pennate taxa expansion is usually bipolar. Once this process finishes, the initial thecae are synthesized. The initial valves may have a modified, more rounded shape than the valves of vegetative cells due to the constraints inside the auxospore and sometimes have a simpler morphology, lacking structures such as spines as in *Melosira* and *Stephanodiscus* (Hasle et al., 1996; Round et al., 1990)

1.4 Resting spores

Diatoms, like some other microorganisms have the capacity to enter a dormant phase in their life cycle when unfavourable environmental conditions arise. Some freshwater planktonic species enter a resting stage, which does not differ morphologically from the vegetative cell except for the thicker cell walls and cytoplasmic content. In most cases however, dormancy is associated with the formation of morphologically distinct cells, called resting spores. Formation of resting spores is a common occurrence in centric diatoms and occurs mostly in species with a distribution in coastal waters and upwelling regions but also at ice fronts (Hargraves, 1986).

Although usually the morphology of the resting spore fairly resembles that of the vegetative cell (e.g. *Coscinodiscus furcatus*; Syvertsen, 1985), some resting spores differ so drastically that they could be classified as a different genus, family or order (e.g. *Chaetoceros* spp.; Hargraves, 1986). Resting spores are generally characterized for their heavily silicified cell walls which usually results in alteration or loss of wall perforations, often coarser areolation and sometimes loss of cingulum bands. There are three main types of resting spores based on the relationship of the mature resting spore to the parent cell i.e. whether the spore is enclosed by the vegetative cell: exogenous, semi-endogenous and endogenous. The same species may produce all types of resting spore as observed in clonal cultures of *Thalassiosira nordenskioeldii* Cleve (Hasle et al., 1996).

Resting spores also occur in fossil species and typically can account for the majority of the fossil assemblage, due to a greater resistance to dissolution (Barron, 1985; Tsukazaki et al., 2013). The resting or vegetative spores of extinct species are often difficult to associate with their initial valve, unless examples of resting cell division are found (e.g. Suto, 2004).

1.5 Application in biostratigraphy and paleoclimatology

Diatoms, like other microfossil groups, are widely employed as biostratigraphic markers for dating stratigraphic sequences, and as datums in the establishment of diatom zonations, which consists in the division, categorizing and characterization of zones of a given studied stratigraphic sequence (often recovered from deep sea drill holes), based on its diatom

associations. These zonations are generally applicable to a broad geographical range but may differ according to latitude and global region. For instance, a diatom zonation for the North Pacific high latitudes (e.g. Yanagisawa and Akiba, 1998) may not be very suitable in the North Atlantic. As in the following pages diatom zones are frequently mentioned, the main zonations of the North Pacific are presented below (figs. 1.2 and 1.3; Akiba, 1986; Barron, 1980; Barron and Gladenkov, 1995; Koizumi, 1973; Schrader, 1973; Yanagisawa and Akiba, 1998). The location of the main drill hole sites considered in this study are also presented below (figs. 1.4 and 1.5).

Diatoms can also be used to better understand the environment and ecological parameters such as sea surface temperature during a given geological time. By knowing the ecology of a given species or group of close related species, this can be used to reconstruct past environments and as a proxy for a given environmental parameter (Sancetta, 1982; von Quillfeldt, 2000, 2001).

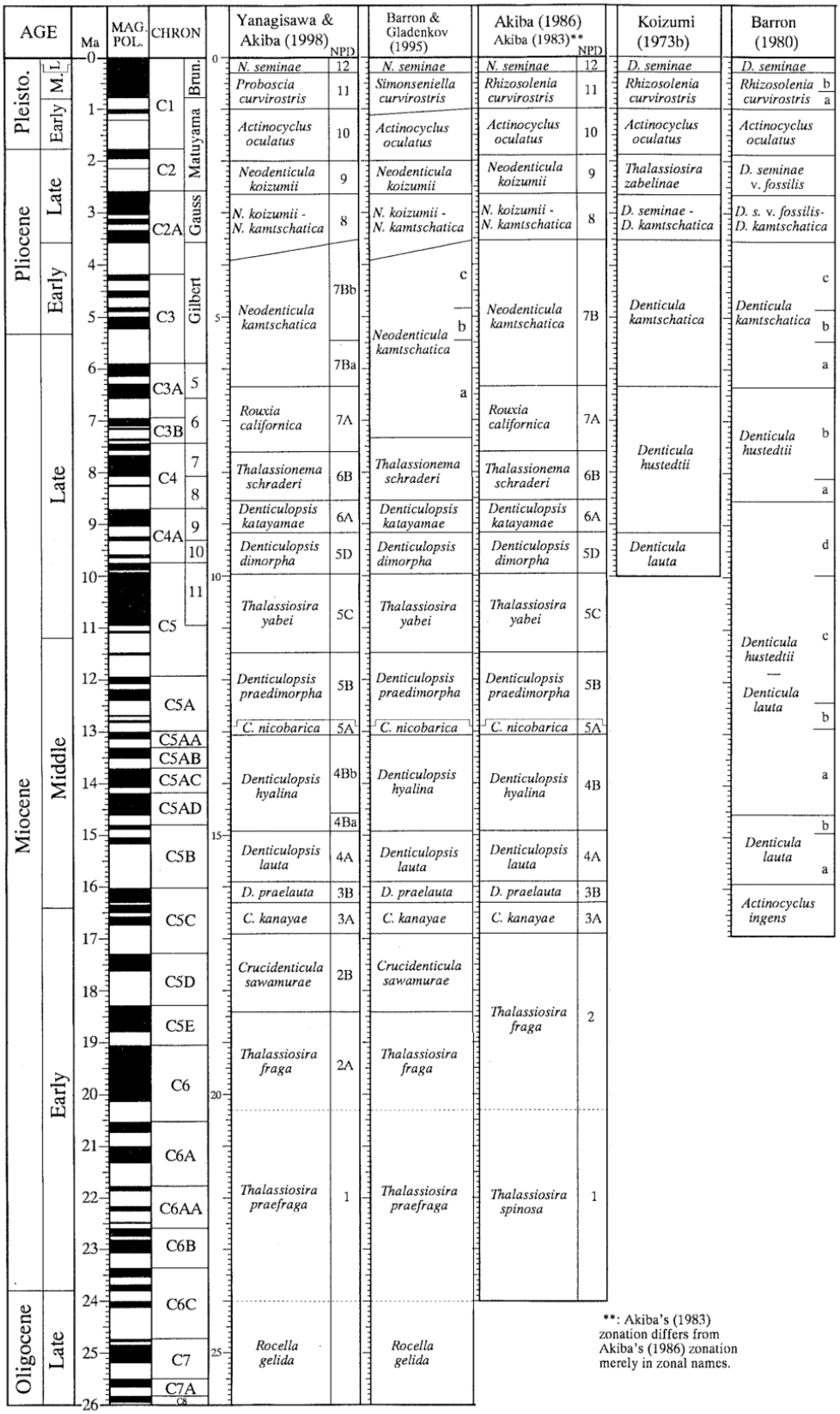

Figure 1.2 - Correlation between high latitude North Pacific diatom zonations. Dotted lines represent indirect correlation between magnetostratigraphy and diatom biohorizons. Adapted from Yanagisawa and Akiba (1998).

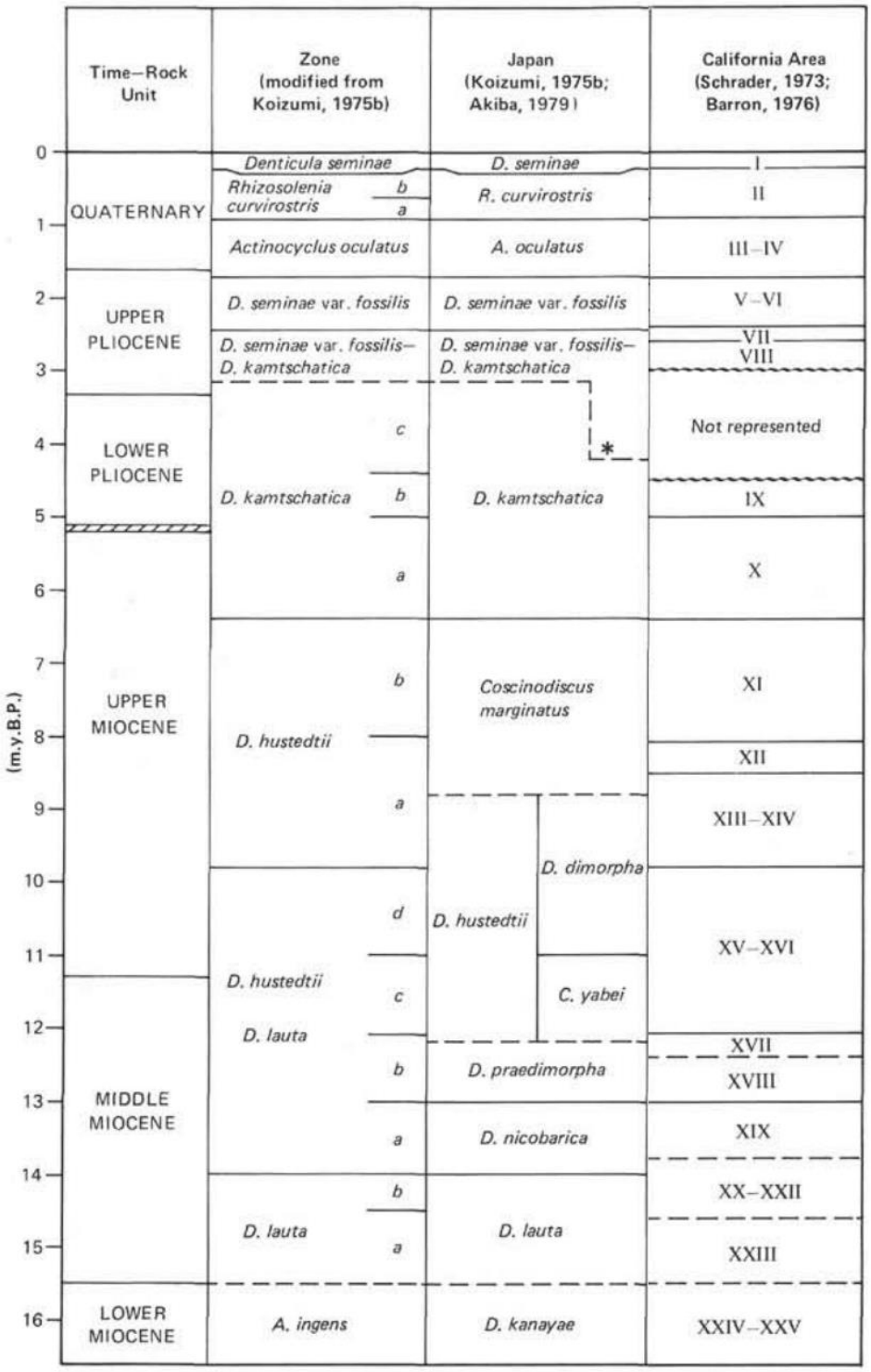

Figure 1.3 - Correlation of the diatom zonation of Schrader (1973) with Barron (1980) and Koizumi (1975b). Adapted from Barron (1980).

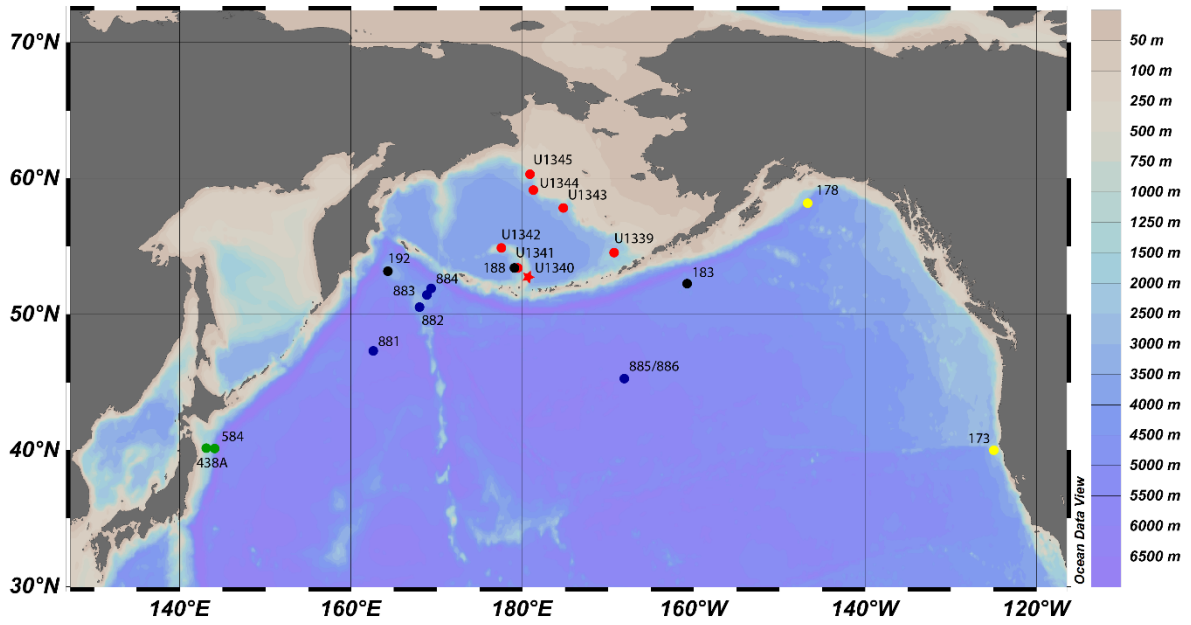

Figure 1.4 - Location of the main Drilling Sites in the North Pacific. Red – IODP Exp. 323; Black – DSDP Leg 19 (Koizumi, 1973); Blue – ODP Leg 145 (Barron and Gladenkov, 1995); Green – Akiba, 1986, Akiba and Yanagisawa, 1986 and Yanagisawa and Akiba, 1998 (DSDP Leg 87 and 57); Yellow – Schrader, 1973 (Leg 18 DSDP). Map generated by Ocean Data View 4.0.

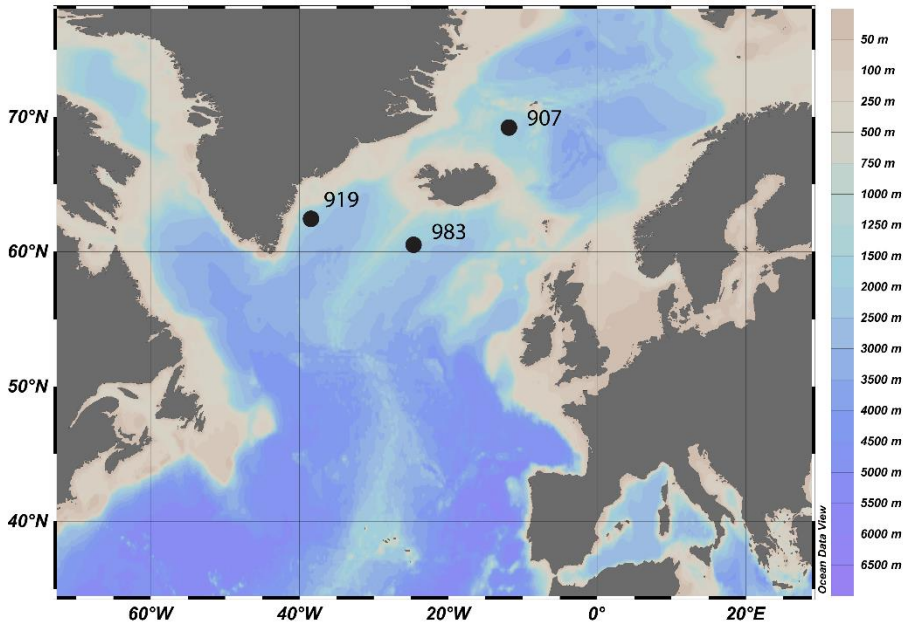

Figure 1.5 - Location of mentioned ODP Sites in the North Atlantic. Map generated by Ocean Data View 4.0.

2 Regional Setting

2.1 Bering Sea Oceanography

The Bering Sea is a marginal sea in the North Pacific with 2.29x10^6 km^2 of surface area, making it the third largest marginal sea in the world. It is bounded by Siberia and Alaska, semi-enclosed by the Aleutian Islands in the South, and connected to the Arctic Ocean through the Bering Strait in the North. The Bering Sea is characterized by its extensive eastern continental shelf, which covers roughly half of its area from northwest to southeast, creating a vast neritic area (<200 m; fig. 2.1). The central and southern area consists of the Aleutian basin (3500 m) with two main structural highs: the Bowers Ridge (which extends from the Aleutian Island arc into the Aleutian Basin), and the Shirshov Ridge (extending from Kamchatka, Siberia). Three major rivers discharge into the Bering Sea waters: Koskokwin and Yukon draining Central Alaska and Anadyr River draining Siberia (Takahashi, 2005).

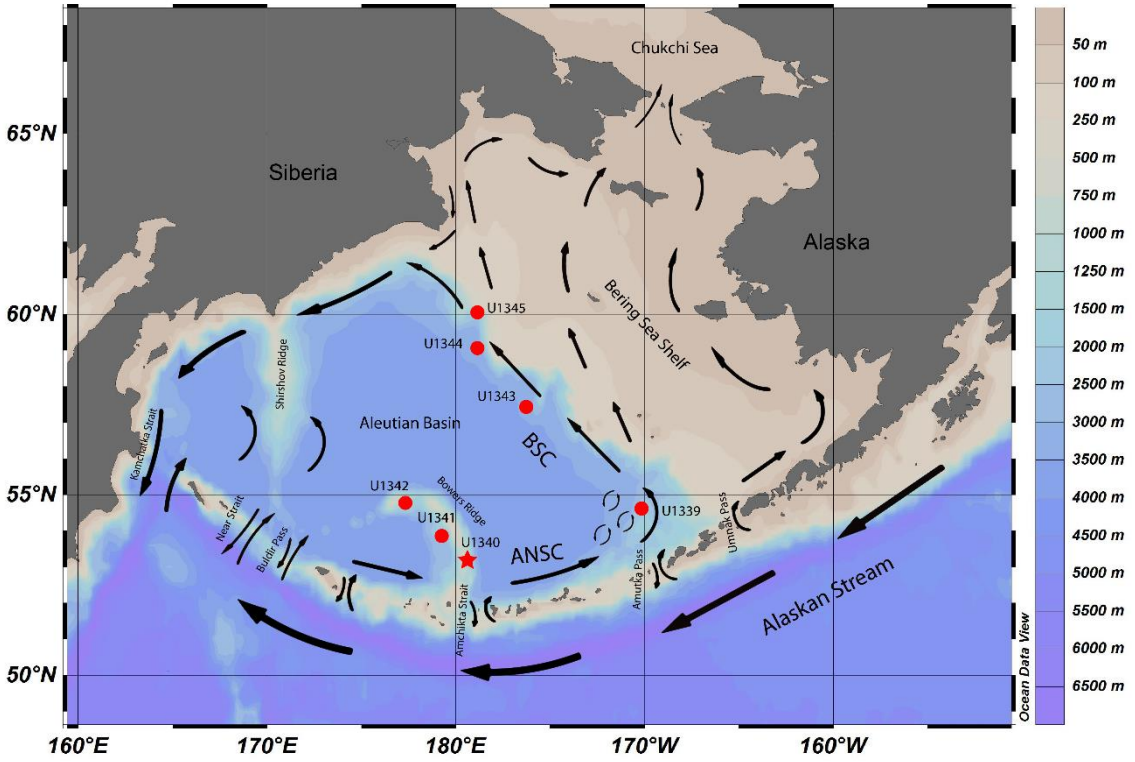

Figure 2.1 - Map of the Bering Sea with the location of Site U1340 (red star) and other sites of the IODP Expedition 323 (red dots). Surface water currents are illustrated by the black arrows. On the right is a scale for the water depth. Map generated by Ocean Data View 4.0.

2.2 Surface Water Currents

The Alaskan Stream (AS) flows westward along the Aleutian Islands and is the main source of water input to the Bering Sea. When combined with part of the Subarctic current joining the northward flow to the Bering Sea, the AS results in a total of $11x10^6$ m^3/s (Ohtani, 1973; Takahashi, 2005). The warm waters of the AS enter the Bering Sea through various Aleutian passes and flow eastward to become the Aleutian North Slope Current (ANSC), then flowing north-westward along the shelf break of the eastern continental shelf as the Bering Slope Current (BSC; fig. 2.1). AS waters enter the Bering Sea mostly through the Amchitka Strait, Near Strait and the Kamchatka Strait while other shallower passes only allow a less significant water exchange (fig. 2.2). The water input is balanced by the outflow, mainly through the Kamchatka Strait. A limited amount of water also flows out unidirectionally through the Bering Strait into the Arctic Ocean. The surface water circulation of the Bering Sea basin follows a large-scale anti-clockwise motion, being thereby commonly described as a cyclonic gyre, except in the Bowers basin where surface water circulation is clockwise. On the eastern Bering Sea shelf water circulation is generally northwestward and despite being important to the Arctic Ocean and global water circulation, it has virtually no influence on the circulation in the Bering Sea basin (Stabeno et al., 1999).

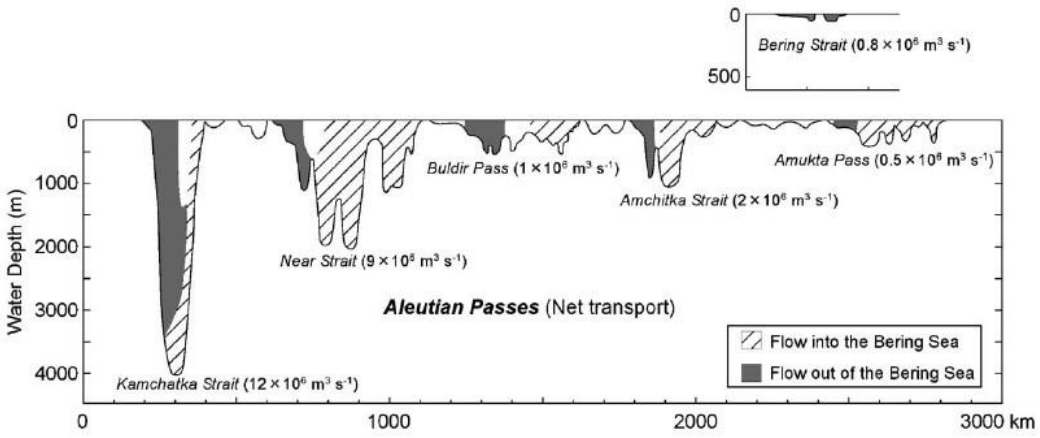

Figure 2.2 - Volume transport in the corresponding main Aleutian Passes and in the Bering Strait. (Takahashi, 2005).

Flow in and out of the Bering Sea has changed in the past as a consequence of glaciations. During glacial intervals, the eustatic sea level drop limited the amount of water exchange through the Aleutian Passes as these became shallower and in some cases closed off with the help of sea ice build-up, diminishing the influence of the AS in the Bering Sea (Katsuki and Takahashi, 2005). Likewise, the Bering Strait, during these periods, became aerially exposed

and closed, cutting the connection to the Arctic Ocean and affecting global water circulation, heat and salt balance (Takahashi, 2005).

2.3 Ecosystem productivity

The Bering Sea is a very productive and rich ecosystem from the basal producers up to the higher trophic levels of the food web. The edge of the Eastern continental shelf is commonly called the Green Belt for being a highly productive area of the Bering Sea, due to upwelling along the Bering Slope, among other physical processes (Springer et al., 1996).

Sea ice is also a fundamental element to ecosystem dynamics and productivity of the Bering Sea. Melting at the ice edge changes the seawater's physical and chemical properties, such as increasing water column stratification and stability, altering water salinity and temperature. These changes in the water column near the ice-edge may enhance and prolong spring blooms, and therefore significantly contribute to the annual primary productivity in the eastern Bering Sea (Alexander and Niebauer, 1981). Sea ice forms seasonally, first in northern Bering Sea in November, moving southward and covering hundreds of kilometres of the Eastern continental shelf, whereas it is rarely present in the southwestern areas (Niebauer et al., 1999). Sea ice is part of the ecology of many diatom species. Epontic diatoms live attached to the underside of sea ice cover or within brine channels in the ice and bloom in the spring, when enough sunlight penetrates the ice. Another type of bloom, named marginal ice zone bloom occurs when sea ice begins to break up on the Bering Sea shelf, releasing nutrients and freshwater from the ice and thereby promoting the bloom (Caisse, 2012).

2.4 Site U1340

Core U1340A was recovered during Expedition 323 of the Integrated Ocean Drilling Project (IODP), which carried extensive drilling throughout the Bering Sea with the aim of studying paleoceanography, and the climate and glaciation history during the Plio-Pleistocene period. Expedition 323 drilled sites on the Bowers Ridge and on the eastern shelf slope and adjacently (fig. 2.1). Site U1340 is located on the eastern flank of the southern part of the Bowers Ridge, at 1295 m water depth, and is more exposed to basin circulation than the neighbouring Site U1341. The Bowers Ridge is greatly influenced by the warm Alaskan Stream waters, which enter the Bering Sea through the adjacent Amchitka Pass and the less significant and more distant Amukta and Buldir passes. Presently, the Bowers Ridge is beyond sea ice extent but it was affected by sea ice or iceberg transportation during glacial periods (e.g. Sancetta and Silvestri, 1986; Katsuki and Takahashi, 2005). There is evidence that during the last glacial maximum, circulation into the Bering Sea was diverted through the western passes of the

Aleutian Islands (e.g. Buldir Pass) due the closure or restriction of the eastern passes (e.g. Amchitka Pass) as consequence of sea level drop. The reduced influence of warmer AS waters resulted in a greater sea ice extent in the eastern Bering Sea, from the Umnak Plateau to the crest of the Bowers Ridge. On the other hand, the western slope of the Bowers Ridge was not substantially covered by sea ice (Katsuki and Takahashi, 2005; Takahashi et al., 2011a).

3 Fossil diatoms of the Bering Sea

3.1 *Proboscia*

Family Probosciaceae Jordan and Ligowski, 2004
Genus *Proboscia* Sundström, 1986

3.1.1 Introduction

Proboscia is a recent genus of rhizosolenioid diatoms which includes a number of species transferred from *Rhizosolenia*, following the taxonomic reviews of this genus (Glezer et al., 1988; Round et al., 1990; Simonsen, 1979; Sundström, 1986; Takahashi et al., 1994). *Rhizosolenia alata* Brightwell was the first species moved to *Proboscia* and was set as the holotype species (Sundström, 1986). Since then several other extinct and extant species of *Rhizosolenia*, some of them sub-taxa of *Rhizosolenia alata* were moved to *Proboscia* (Takahashi et al., 1994).

Rhizosolenioid is a general term used for diatoms of the family Rhizosoleniaceae and historically related taxa such as the recent family Probosciaceae. Generally, rhizosolenioid diatoms are adapted to stratified waters with a strong nutricline and thermocline, as they are able to vertically migrate between the nutrient rich deeper layers of the water column and the euphotic zone. Some taxa within the *Rhizosolenia* genus, have been found to host an endosymbiotic Nitrogen-fixing cyanobacteria. Species with this ecology are commonly called shade flora and include other species such as: *Thalassiothrix spp.*, *Coscinodiscus spp.*, *Stephanopyxis palmeriana* and *Proboscia alata*. The cumulative production by shade flora diatoms during periods of stratified waters, generally during summer, and subsequent sinking and sedimentation in autumn/winter (i.e. “Fall dump”), when mixing breaks down the nutricline, accounts for a significant proportion of export production, comparable or even superior to that yielded by spring blooms (Kemp et al., 2000). The sedimentation of shade flora diatoms may form laminae in the sediments and thus may also be referred to as mat-forming species (Kemp et al., 2000; Sukhanova et al., 2006).

3.1.2 Morphology of *Proboscia*

Proboscia, *Rhizosolenia* and other rhizosolenioid diatoms share many common morphologic features (fig. 3.1). The cells are cylindrical with unipolar valve symmetry. The girdle is composed of several repeating elements i.e. segments, bands or copula. The distal ends of the frustule bear special structures involved in forming chains of frustules namely, the external process - a pointy structure on the tip of the distal end of the valve. Species of *Proboscia*, which formerly belonged to the genus *Rhizosolenia* - a genus with a typical external process - lack this structure, and possess a proboscis instead. The proboscis is a tubular extension of the valve,

often curved, distinct from the external process, and is diagnostic of *Proboscia* (Hasle et al., 1996; Medlin and Priddle, 1990).

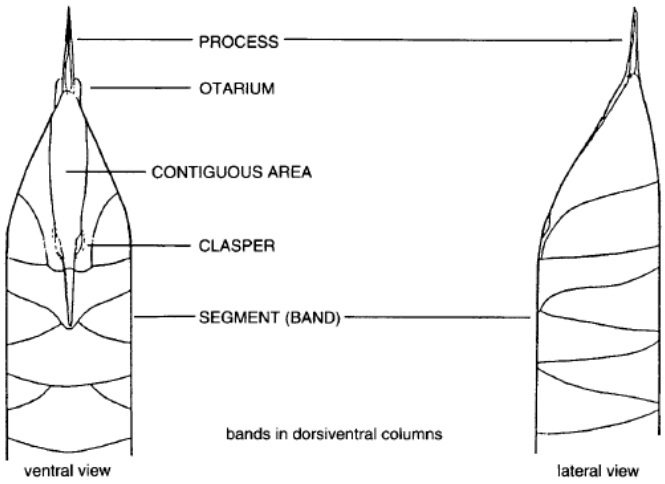

Figure 3.1 - General morphology of *Rhizosolenia* spp. (Hasle et al., 1996).

The frustule of *Proboscia* is cylindrical and the valves are subconical. The ends of the valves lack the external process and terminate into the tubular structure known as proboscis (fig. 3.2). The distal end of the proboscis usually bears spinulae (i.e. short spines; e.g. *P. alata*) and/or spines (*P. curvirostris* and *P. barboi*). Many species form chains of individual cells by attaching the terminal end of the proboscis to the groove formed by clasper-like structures of the host cell and thereby binding to its ventral side (i.e. the contiguous area). Species such as *P. subarctica* (= *Rhizosolenia alata* Brightwell f. *curvirostris* Gran, 1900), not bearing these morphologic features, characteristic of chain-forming species, are either solitary or form chains through other mechanisms (Hasle et al., 1996; Takahashi et al., 1994). In fossil species, the basal portion of the valve is missing; therefore it is not possible to know whether they formed chains as do extant species, although alternative mechanisms may have been present. Auxospores are terminal, in contrast to the lateral position of auxospores of *Rhizosolenia*. The proboscis usually bears a longitudinal slit on the dorsal side at the distal end which, in extant species is longer and closer to the tip in comparison to fossil species.

Extant species are also characterized for having spring and winter forms. In the latter, the proboscis is much longer and the valve may lack claspers. The winter form proboscis of extant species (e.g. *P. truncata*, 30 µm; *P. subarctica* 70 µm), are significantly shorter than the proboscis of fossil species which is usually longer than 100 µm (Jordan and Priddle, 1991; Takahashi et al., 1994).

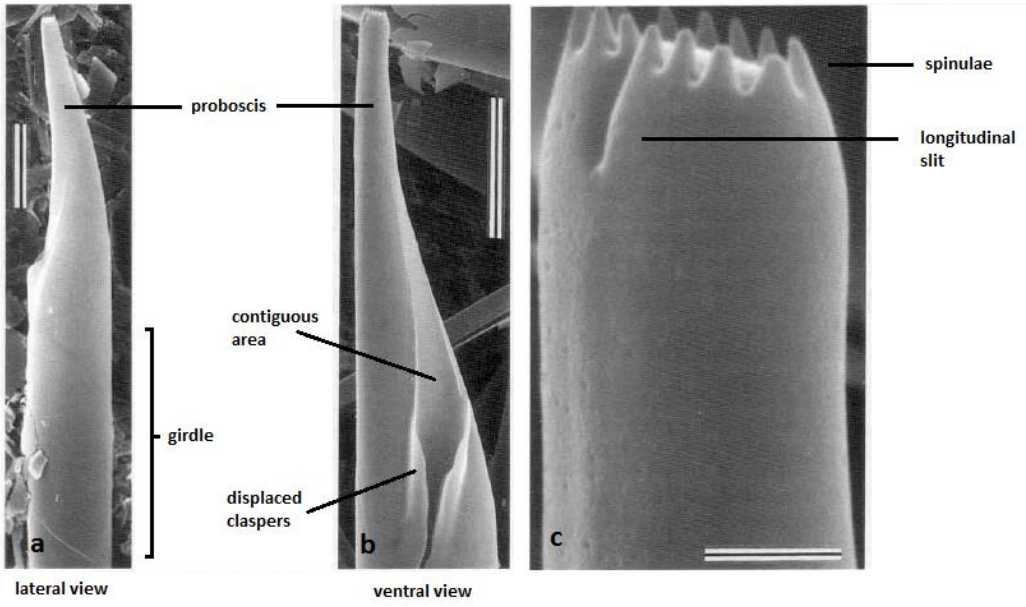

Figure 3.2 – SEM images of *P. alata*. Scale bar: a, b - 10 µm; c – 1 µm. Adapted from Takahashi et al. (1994)

3.1.3 Ecology

Extant *Proboscia* have a wide distribution, with species distributed from the subarctic (e.g. *P. subarctica*) and antarctic (e.g. *P. truncata* and *P. inermis*) to tropical environments (e.g. *P. indica*; Hernández-Becerril, 1995; Jordan and Priddle, 1991; Sunesen and Sar, 2007). *P. alata* is common in polar waters but also found in tropical and subtropical waters (Hernández-Becerril, 1995; Jordan and Ligowski, 2004) although this widespread distribution may be due to *P. alata* actually being a complex of cryptic species (Jordan and Ligowski, 2004; Sundström, 1986). *P. alata* has been considered a key "fall dump" species in the Gulf of Alaska, and in the Walvis Ridge, South Atlantic (Kemp et al., 2000; Takahashi et al., 1994; Treppke et al., 1996). In the Bering Sea shelf, *P. alata* is one of the dominant contributors to phytoplankton biomass and abundance from late May to early September, with the highest peak in August, during a period typified by stratified waters. However, in subtropical/tropical regions such the Arabian Sea and off the Somalian coast, *P. alata* along with *Rhiziosolenia spp*. is a dominant species prior to or early in the upwelling season (Gordon and Seckbach, 2012; Kohning et al., 2001; Smith, 2001). The ability to adjust their buoyancy allows these species to migrate to deeper layers bellow the euphotic zone and reach the nutrients during the onset of upwelling events, before other species (Koning et al., 2001; Villareal, 1988).

The seasonal life cycle of *P. subarctia* on the other hand differs from that of *P. alata*. Its flux peak, studied at the same stations as *P. alata* occurs during spring and slowly decreases

towards winter, indicating that this species proliferates under high nutrient and low light conditions (Takahashi et al., 1994), and so does not appear to fit in the fall dump annual cycle.

3.1.4 *Proboscia barboi* and *Proboscia curvirostris*: phylogenetic relation

Proboscia extends back from Late Cretaceous to the present day. Taxa with long proboscis, particularly the winter forms, bear the closest resemblance to the fossil taxa.

P. barboi and *P. curvirostris* were two former Cenozoic *Rhizosolenia* extinct species. Akiba and Yanagisawa (1986) assumed from the strong morphologic similarities, that *P. barboi* which proceeded from *P. praebarboi*, evolved into *P. curvirostris*, thereby forming a continuous evolutionary lineage. However, Jordan and Priddle (1991) remark that the existence of previous species with curved probosces and bearing terminal spines argue against the hypothesis of that evolutionary sequence. Furthermore, Hajós (1976) suggests that *P. interposita* is an intermediate species between *P. cretacea* and *P. curvirostris* and shows "close affinity" with the latter species. Therefore, the evolutionary hypothesis presented by Akiba and Yanagisawa (1986) is not consensual and needs more evidence.

It has also been remarked in the literature that *P. subarctica,* whose morphology is quite different from other extant species namely due to the absence of contiguous area and claspers, bears a striking similarity to *P. barboi* and *P. curvirostris* (Donahue, 1970; Jordan and Priddle, 1991; Takahashi et al., 1994).

3.2 *Proboscia curvirostris* (Jousé) Jordan and Priddle, 1991

Original description: Jousé, 1968, p. 19, pl. 3, fig. 2.
Synonymy: *Rhizosolenia curvirostris,* Akiba, 1986; Akiba and Yanagisawa, 1986

3.2.1 Geographic distribution and stratigraphic range

P. curvirostris is an extinct species found in Pleistocene sediments of both the North Atlantic and North Pacific with a mid to high latitude distribution. Only the proboscis of the valve is preserved in the sediments. Being a dissolution-resistant species and having a short stratigraphic span makes it a good Pleistocene biostratigraphic marker.

In the North Pacific, *P. curvirostris* makes its evolutionary appearance in NPD10 (fig. 1.2), at 1.37-1.42 in the Bowers Ridge (IODP U1341; Onodera et al., 2013), 1.58 Ma in the Western Subarctic (ODP Sites 881 to 884 and 887; Barron and Gladenkov, 1995), and 1.7 Ma on the Bering Slope (IODP Site U1343; Teraishi et al., 2013). In the North Atlantic, its FO is also observed at ODP Site 983 around the same age at 1.53 Ma (Koç et al., 1999), which means this FO is relatively synchronous between the two oceans.

The LO of *P. curvirostris* defines the top of the *Proboscia curvirostris* Zone (NPD11) and varies between 0.26 and 0.35 in the North Pacific although it reveals some diachroneity according to location (Barron and Gladenkov, 1995; Koizumi and Tanimura, 1985; Yanagisawa and Akiba, 1998; Onodera et al., 2013; Teraishi et al., 2013). In Northernmost Emperor Seamount it is dated at 0.26 Ma (Katsuki and Takahashi, unpublished data, *in* Takahashi et al., 2011b) and in the Bowers Ridge at 0.28 Ma +-0.02 (IODP Site U1341; Onodera et al., 2013; fig. 3.4). The extinction of *P. curvirostris* and the subsequent replacement by the cold water species *R. hebetata* Bailey in the North Pacific is related to the Mid-Brunhes event and a transition to more extreme glacial conditions (Jansen et al., 1986; Sancetta and Silvestri, 1984).

In the North Atlantic, its extinction is latitudinally diachronous through MIS 9-8. It first disappeared in the northern areas which are more sensitive to climatic forcing at 0.31 Ma (Irminger Basin, ODP 919) and survived in the mid latitudes, approximately 40°N until 0.26 Ma. The overlap in age between the North Atlantic and North Pacific strongly suggests that the LO of *P. curvirostris* is relatively synchronous in both oceans (Koç et al., 2001).

3.2.2 Description

The proboscis of *P. curvirostris* consists of a long hollow tube, cylindrical in shape and is characterized by a conspicuous dorsal spine (i.e. dorsal fin) with a flat triangular shape at or near the maximum curvature of the valve, which is 80° to 160° (fig. 3.3; Donahue, 1970). The distal end of the valve terminates with a flattened top plate on which two spines are displayed: the dorsal spine nearly parallel to the top plate and the ventral spine perpendicular to it. The top plate is elliptical in outline and the rest of its periphery bears spinulae. The valve is hyaline except for two kinds of striations and a small slit only discernible by SEM: several long longitudinal rows of striae lining the dorsal and ventral sides, terminating at a short distance from the apex and several rows of short longitudinal striae restricted to the apex region, positioned between the longer rows of striae. Like many extant *Proboscia* species (e.g. *P. alata*, *P. eumorpha* and *P. subarctica*; Takahashi et al., 1994), the valve displays a short longitudinal slit near the apex. The dorsal fin is diagnostic and distinguishes this species from *P. barboi* (Akiba and Yanagisawa, 1986; Jordan and Priddle, 1991).

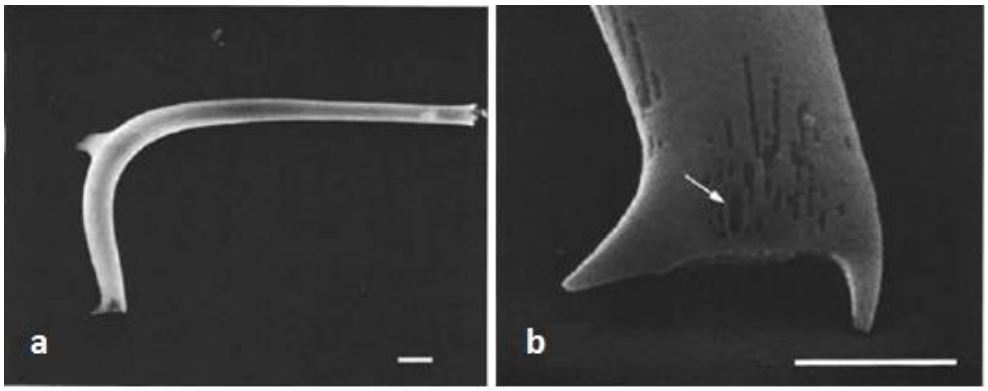

Figure 3.3 – SEM images of *Proboscia curvirostris* (a) and its distal end (b). Arrow indicates longitudinal slit. Scale bar: a - 10 µm; b - 5 µm (Akiba and Yanagisawa, 1986).

3.3 *Proboscia barboi* (Brun) Jordan and Priddle, 1991

Original description: Brun, 1894, p. 87, pl.5, figs. 16-17, 23 as *Pyxilla* (R*hizosolenia*?) *barboi* Brun. Synonymy: *Rhizosolenia curvirostris* var. *inermis* Jousé, 1971

3.3.1 Geographic distribution and biostratigraphy

P. barboi is an extinct species found in Miocene-Pleistocene sediments of both the North Atlantic and North Pacific with a high- to middle-latitude distribution. Like *P. curvirostris*, this species is known from the valves' probosces that are preserved on the sediments.

In the North Pacific, the FO of *P. barboi* goes back to the Upper Middle Miocene (NPD5B; Akiba and Yanagisawa, 1986). Contrary to *P. curvirostris*, the LO of *P. barboi* is more variable, depending on location (fig. 3.4). The LO of *P. barboi* is divided into two main ages: close to 0.3 Ma, at the same time *P. curvirostris* disappears or close to the FO *P. curvirostris* (1-2 Ma). In many locations such as the Bowers Ridge (IODP Site U1341), *P. barboi* disappears a little earlier than *P. curvirostris*, at 0.42-0.47 Ma (Onodera et al., 2013), at IODP Site U1343 (Teraishi et al., 2013) the LO is roughly at 0.6 Ma (age corresponding to 140 m depth; fig. 4.2), and in the Northwest Pacific, off Japan's east coast, it occurs at the same age as *P. curvirostris* (0.3 Ma; Yanagisawa and Akiba, 1998). However, the LO of P. barboi at Site U1343 was determined on supplementary data of Teraishi et al. (2013), and may not be robust, as the occurrences of *P. barboi*, become scant and sparse from 1.6 Ma upwards (380 m depth; fig. 5.2). This species and its LO are never mentioned in Teraishi et al. (2013). In the Alaskan Gulf and off the coast of Northern California, *P. barboi* disappears at the same age as *P. curvirostris* appears. The synchronous LO of *P. barboi* and FO of *P. curvirostris* (together with the LO of *Thalassiosira antiqua*), were used to define the base of NPD Zone IV (Schrader, 1973). The compiled stratigraphic ranges for the Bering Sea and Northern Pacific Ocean (DSDP Sites 183 to 192, Leg 19; Koizumi, 1973), mark the LO of *P. barboi* near the LO of *P. curvirostris* (top of *Rhizosolenia*

curvirostris zone, ~0.3 Ma). Nevertheless, on the South side of the Aleutian Islands Arc (Sites 183 and 192) and on the Western flank of Bowers Ridge (Site 188), the LO of *P. barboi* approximately matches the FO of *P. curvirostris* near the top, ~1 Ma; bottom, ~2 Ma; and middle, ~1.5 Ma of *Actinocyclus oculatus* zone, correspondingly.It is odd that while sites 188 and U1341 are both located in the same region (Western flank of the Bowers Ridge), they have such a large age discrepancy on the LO of *P. barboi*.

In the Atlantic Ocean on the Iceland Plateau (Site 907), *P. barboi* disappears at 3.3 Ma, approximately 3 Ma earlier than the extinction of *P. curvirostris* (Koç and Scherer, 1996).

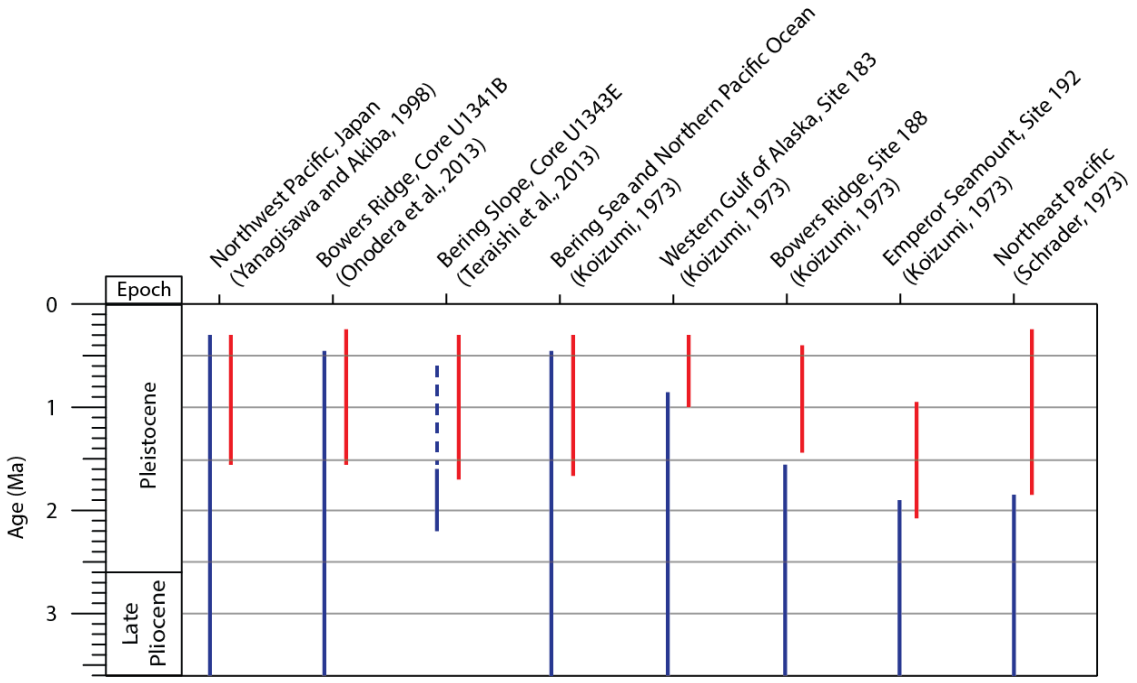

Figure 3.4 – Stratigraphic ranges of *P. barboi* and *P. curviostris* in several sites of the North Pacific. *P. barboi* either disappears near the LO or FO of *P. curvirostris*, varying with site. Dashed line indicates scarce occurrences. Blue – *P. barboi*; Red – *P. curvirostris*.

3.3.2 Description

Proboscia barboi is almost identical to *P. curvirostris,* the main differences being its bigger and bulkier size, the less marked curvature and most importantly, the lack of dorsal fin (fig. 3.5). The distal end of the tube bears two large spines. In the SEM the top plate of the distal end is ovate to elliptical in outline with one large spine at each pole and spinulae on the rest of the periphery. In many cases, the orientation of one of the spines makes 90° with the distal end and the other extends distally. The morphologic ultrastructural features (the longitudinal rows of striae and the longitudinal slit) described for *P. curvirostris* are also present in *P. barboi* and equally applicable (Akiba and Yanagisawa, 1986).

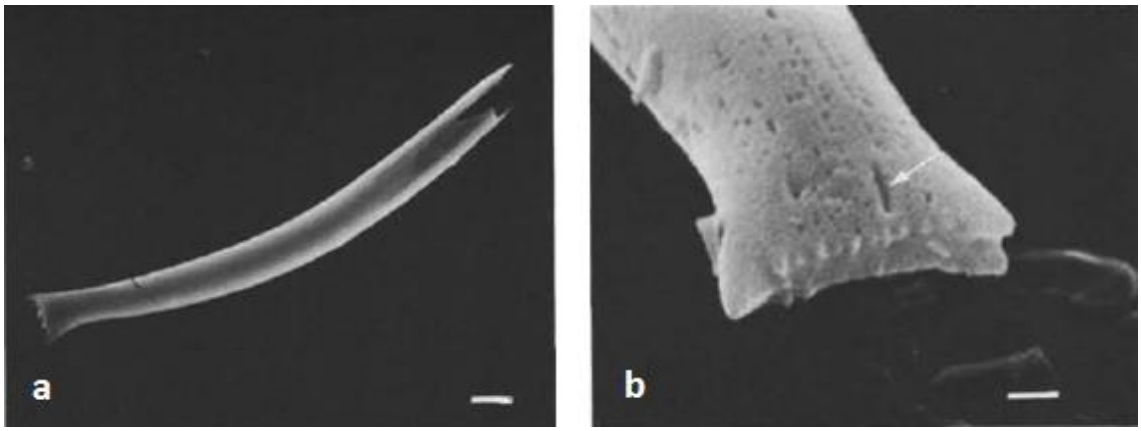

Figure 3.5 – SEM images of *Proboscia barboi* (a) and its distal end (b). Arrow indicates longitudinal slit. Scale bar: a – 5 µm; b – 1 µm (Akiba and Yanagisawa, 1986).

3.4 Thalassiosira

Family Thalassiosiraceae (Lebour) Hasle, 1973
Genus *Thalassiosira* (Cleve) Hasle, 1973

3.4.1 Introduction

Thalassiosira is a large genus of marine diatoms, with more than 100 species. Cells are discoid or cylindrical and form chains by connecting organic threads. *Thalassiosira* species are found in a wide variety of environmental settings including sea ice, upwelling zones, highly stratified waters, cold, and warm waters. The type species is *Thalassiosira nordenskioeldii* Cleve, a species part of the spring bloom in the marginal ice zone (Caisse, 2012; von Quillfeldt et al., 2003).

The classification of the genus and its species is mostly based on the strutted, occluded and labiate processes present on the valve face, that are either isolated or in ring formations, and are best observed by electron microscopy. These structures are openings in the valve face consisting of tubes that differ in their internal structure. The first two mentioned structures are diagnostic of Thalassiosiraceae. The number, arrangement and position of these structures are important characters of the genus' taxonomy, while the valve size and areolae density are not as taxonomically diagnostic as they vary considerably within the species rank. The strutted processes are involved in colony formation by extruding threads that link frustules together (Hasle et al., 1996; Makarova, 1980). Resting spores occur in *Thalassiosira* and have been fairly well studied (Hasle et al., 1996).

3.4.2 *Thalassiosira jouseae* Akiba, 1986

Description: Akiba, 1986, p. 440, pl. 6, figs. 8-10

Synonym: *Thalassiosira nidulus* (Tempère and Brun) Jousé, 1961, p. 63, pl. 3, figs. 4-5; *Thalassiosira nidulus* (Tempère and Brun) Jousé var. *nidulus* (nomen nudum), Barron, 1980a, p. 673, pl. 6, fig. 5.

3.4.2.1 Geographic distribution and biostratigraphy

Thalassiosira jouseae is a species with a mid to high latitude distribution in the Pacific and Atlantic Oceans. It appears in the uppermost Miocene (Yanagisawa and Akiba, 1998), and becomes extinct approximately at 0.3 Ma in the North Pacific (fig. 3.8), the same age as *P. curvirostris* (Onodera et al., 2013; Teraishi et al., 2013; Yanagisawa and Akiba, 1998). Its LO is a secondary biohorizon defining the top of zone NPD11 (Akiba, 1986), and is synchronous in both North Pacific and North Atlantic Oceans (Koç et al., 2001).

3.4.2.2 Description

T. jouseae (fig. 3.6, 3.7b and 3.9) has a circular valve with 9-29 µm in diameter. The valve is sparsely areolated in the central part of the valve face. Areolae are quadrangular, more or less isolated from each other, 8-10 areolae in 10 µm. The most distinguishing feature of the valve is the conspicuous sub-marginal tapering spines that form a crown-like structure by uniting their basal parts (Akiba, 1986). These structures correspond to the marginal strutted processes.

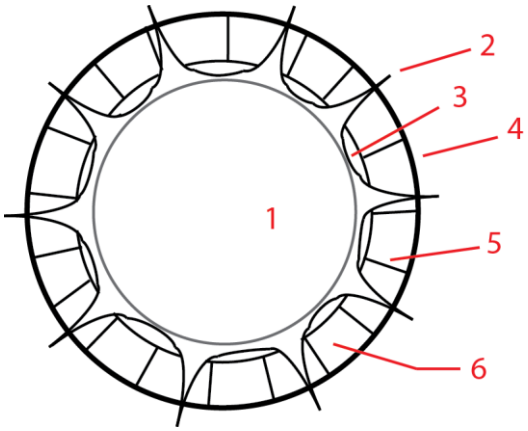

Figure 3.6 - Schematics of *Thalassiosira jouseae* (valve view). Legend: 1 – valve face; 2 – sub-marginal spine; 3 – base of sub-marginal spines; 4 – marginal rim; 5 – marginal ribs; 6 – margin.

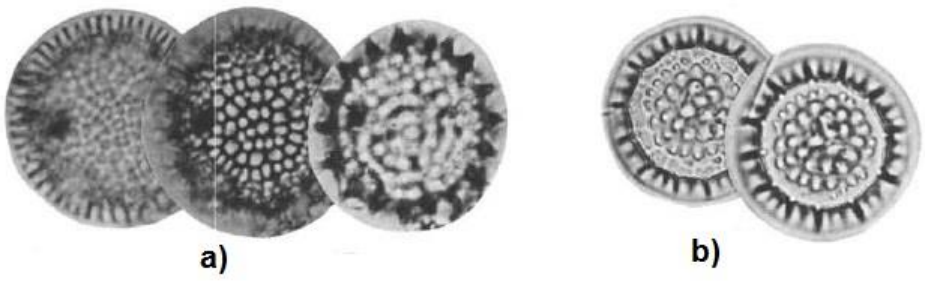

Figure 3.7 - Holotypes of *T. nidulus* (Tempère and Brun) Jousé (a) and *T. jouseae* Akiba (b). Magnification 1500x. (Akiba, 1986).

3.4.2.3 *Thalassiosira nidulus*: taxonomy and biostratigraphy

Akiba (1986) discovered and described *T. jouseae* based on specimens that had been assigned to *Thalassiosira nidulus* by Jousé (1961). The latter species has an older taxonomic history. It was originally described as *Stephanopyxis nidulus* Tempère and Brun in Brun and Tempère (1889), and then transferred to the genus *Thalassiosira* by Jousé (1961). Akiba (1986) places *T. nidulus* (Tempère and Brun) Jousé 1961, as a synonym of *T. jouseae*. However, the author is only referring to *T. nidulus* of plate 3, figs. 4-5 of Jousé (1961) and not the other specimens (plate 1, figs. 3-4). Therefore, the taxon *T. nidulus* represents a real species and should not be used interchangeably with *T. jouseae*.

T. nidulus (fig. 3.7a and 3.10) appears in the Upper Miocene (DSDP Hole 438A; Akiba, 1986) and in North Atlantic in the Lower Pliocene (ODP Site 907; Koç and Scherer, 1996). The LO of *T. nidulus* is synchronous with that of *T. jouseae* although from the end of the Miocene epoch onwards its occurrences become rare or sporadic (DSDP Hole 584; Akiba, 1986). In the North Atlantic, *T. nidulus* has a shorter stratigraphic range, within the lower-middle Pliocene (ODP Site 907; Koç and Scherer, 1996).

Barron (1980) actually seems to precede Akiba (1986) by distinguishing a variation "nidulus" of *T. nidulus* (Tempère and Brun) Jousé from the Pacific subarctic, although not accompanied with a description. Akiba (1986) listed said variation as a synonym of *T. jouseae*. Indeed *T. nidulus var. nidulus* Barron looks identical to *T. jouseae* and both LOs match very closely, defining the top of Zone *Rhizosolenia*/*Proboscia curvirostris* (Barron, 1980; Yanagisawa and Akiba, 1998). Barron (1980) also considers *T. nidulus* of Schrader (1973, pl. 11, figs. 1-7) as *T. nidulus var. nidulus* which would imply that *T. nidulus* (Schrader, 1973) are actually *T. jouseae*. However, Akiba (1986) does not include *T. nidulus* (Schrader, 1973) in the synonymy of *T. jouseae*, possibly because of the different stratigraphic ranges.

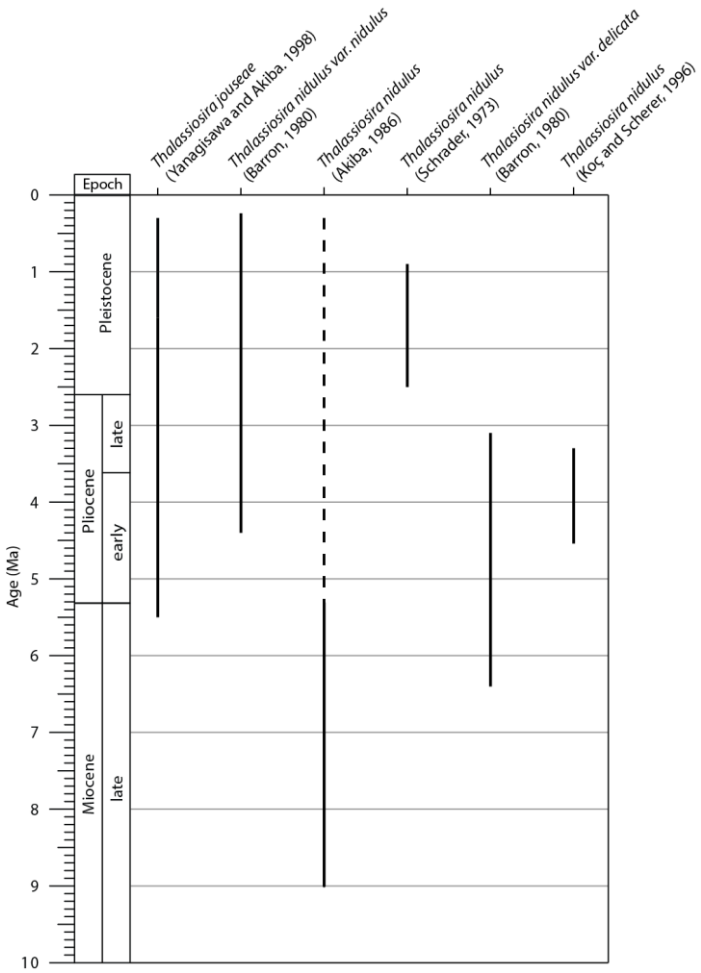

Figure 3.8 - Stratigraphic ranges of *T. jouseae*, *T. nidulus* and variations in North Pacific Sub-arctic, and *T. nidulus* (Koç and Scherer, 1996) in North Atlantic Sub-arctic. Note: *T. nidulus* var. *nidulus* = *T. jouseae* Akiba; *T. nidulus* var. *delicata* = *Thalassiosira delicata* Akiba. Dashed line indicates rare to sporadic occurrences.

The LO of *T. nidulus* (Schrader, 1973) was established in lower NPD Zone III (0.92-1.3 Ma) somewhat earlier than the LO of *Rhizosolenia curvirostris* which defines the top of NPD Zone II (Schrader, 1973), whereas in the literature the LO of *T. jouseae* occurs later (~0.3) and is coincident with the LO of *P. curvirostris* (fig. 3.8).

3.4.3.3 Distinguishing *Thalassiosira jouseae* from *Thalassiosira nidulus*

The original description of *T. nidulus* (Jousé, 1961) is not accessible by most means, which complicates its recognition and contributes to the confusion with *T. jouseae*. Nevertheless, Akiba (1986) remarks that *T. jouseae* is distinguished from *T. nidulus* by the "united basal parts of sub-marginal spines, smaller valve, and sparser areolae on valve face" (fig.3.7b; Akiba, 1986).

By observing the SEM images of *T. jouseae* (Koç et al., 1999; DSDP Site 983A, late Pliocene) and *T. nidulus* (Koç and Scherer, 1996; ODP Site 907A, late Pliocene) it is possible to

notice significant differences between them. The former images show a *T. jouseae* specimen (fig. 3.9; 10 µm valve diameter) with a convex valve face and areolation restricted to the central area, leaving the periphery hyaline. The striated margin displays the ribs connecting to the marginal rim. On the other hand, in the *T. nidulus* specimen (fig. 3.10; 17 µm valve diameter) the valve face is flat and the areolation covers all of its area till the base of the sub-marginal spines. The areolae are also arranged closer to each other. The marginal rim seems to be missing, leaving only the ribs. The sub-marginal spines of *T. nidulus* do not seem to have united basal parts and thus can be said to have separate spines, whereas the spines of *T. jouseae* have united basal parts as noted by Akiba (1986).

In the TEM images of Akiba (1986), the holotype of *T. nidulus* is densely areolated, with contiguous irregularly sized areolae covering all of the valve face and arranged in (imperfect) concentric rows (fig. 3.7a).

Although *T. jouseae* and *T. nidulus* are fairly distinguishable on these SEM images, the identification of *T. jouseae* on LM is often ambiguous. In the morphology chapter, *T. jouseae* and *T. nidulus* are described based on specimens from U1340A samples of the Pleistocene.

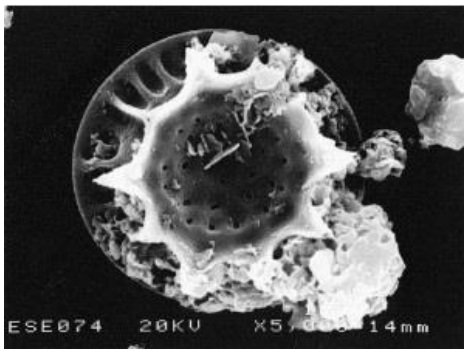

Figure 3.9 - SEM image of *T. jouseae* in valve view (Koç et al., 1999).

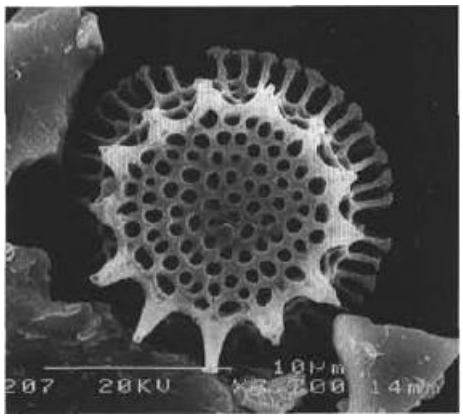

Figure 3.10 - SEM image of *T. nidulus* in valve view (Koç and Scherer, 1996).

4 Methodology

4.1 Samples

The studied core samples were obtained from International Drilling Program (IODP) repository from selected intervals from Core U1340A. The Site is located at 53°24.0008' N, 179°31.2973' W, on the eastern flank of the southern part of Bowers Ridge in the Bering (fig. 2.1). Four holes were drilled during IODP Expedition 323 in 2009, and cored with the advanced piston (APC) and extended core barrel (XCB) coring systems at a water depth of 1294.7 m. All analysed samples are from Hole U1340A, which was cored to 604.6 m drilling depth below seafloor (DSF) using both APC and XCB coring systems. Diatom biostratigraphy at Site U1340 was based on core catcher samples from Hole A and a biostratigraphic zonation was constructed until the lowermost Pliocene, ca. 5 Mya (Subzone NPD 7Bb; Yanagisawa and Akiba, 1998; Takahashi et al., 2011b). The age models of Site U1340 (hole A) and other IODP Exp. 323 Sites are presented bellow (fig. 4.1 and 4.2).

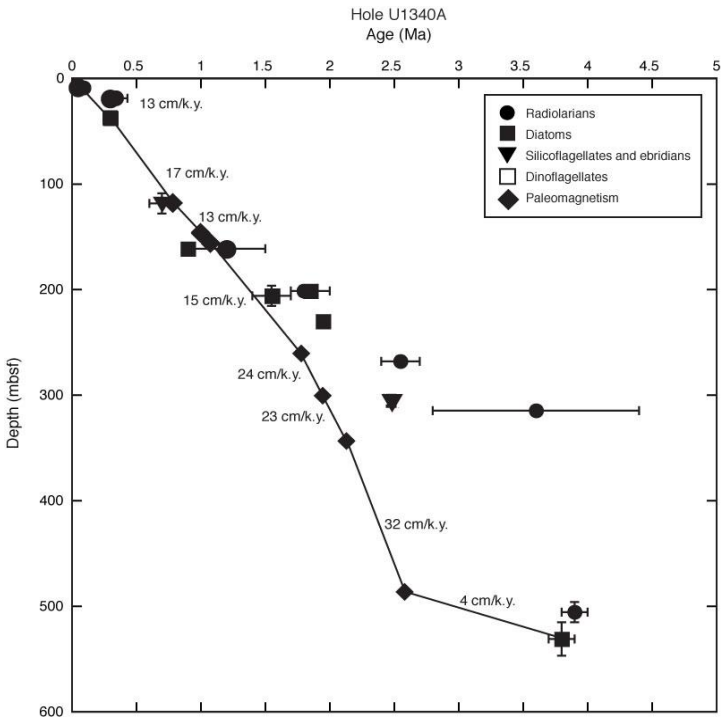

Figure 4.1 - Age-depth plot for core U1340A showing biostratigraphic datums based on diatoms and other microfossil groups. Paleomagnetic events are also shown. (Takahashi et al., 2011b).

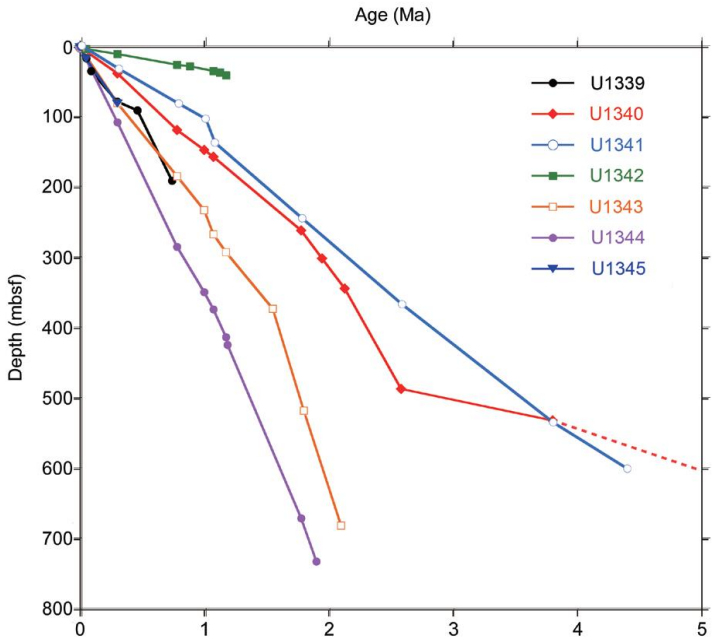

Figure 4.2 - Age-depth plot for Sites U1339-U1345 (Takahashi et al., 2011a).

4.2 Method

In order to study the biostratigraphy and morphology of *P. barboi*, *P. curvirostris* and *T. jouseae*, a total of 43 samples were used (3H-CC, 23.12 m to 28H-3, 238.55 m; table 4.1), covering an age interval from 0.18 to 1.63 Ma, roughly encompassing the stratigraphic span of *P. curvirostris*. The observed samples and slides are the same as the ones previously used for the biostratigraphy of core U1340A (Stroynowski et al., 2015). Counts of the three mentioned species were performed on light microscope (LM; Nikon eclipse 80i) under x1000 (or under x600, when suitable) magnification, by running transects on the first slide of each sample.

The productivity of each species was calculated by applying the following formula (Abrantes et al., 2005):

No. valves/gram = $((N*(S/s))*(V/v))/W$

N - number of valves counted
S - area of the evaporation tray (mm^2)
S - observed area of the slide (mm^2)
V - volume of solution in the beaker (ml)
V - aliquot or volume of solution put into the evaporation tray (ml)
W - weight of raw sample (g)

Radius (slide) = 10 mm
Radius (evaporation tray) = 55 mm

The area observed on each slide was calculated considering the shape of each transect as approximately that of a rectangle. Thus the observed area is the sum of the areas of all transects run on the slide. The height of one transect is equal to the diameter of the field of view (FOV), which depends of the microscope used. The FOV diameters (D) of each magnification are: D_{1000x} = 0.22 mm; D_{600x} = 0.40 mm; D_{400x} = 0.61 mm

Table 4.1 - Area (mm^2) observed for each sample. Note: counts of *T. jouseae* on samples 24H-5 and 25H-5 were performed on 40.66 mm^2 and 39.23 mm^2 respectively.

Core U1340A sample #	Mid-depth (cm)	Depth (Mid CSF m)	Area observed (mm^2)
3H-CC	0.5	23.12	314.16
4H-3	135.5	25.75	314.16
4H-5	135.5	28.75	314.16
4H-CC	0.5	32.56	628.32
5H-CC	0.5	42.13	314.16
6H-CC	0.5	51.68	314.16
7H-CC	0.5	61.2	314.16
8H-3	135.5	65.25	314.16
8H-5	135.5	68.25	314.16
8-CC	0.5	70.69	314.16
9H-3	135.5	75.95	314.16
9H-5	135.5	77.75	314.16
9H-CC	0.5	80.11	40.46
10H-3	135.5	84.26	314.16
10H-5	135.5	87.25	40.06
10H-CC	0.5	89.63	157.08
11H-5	135.5	96.75	34.21
11H-CC	0.5	99.17	38.72
12H-CC	0.5	108.61	37.22
13H-5	135.5	115.75	37.55
13H-CC	0.5	118.06	36.28
14H-3	105.5	121.95	40.94
14H-6	135.5	126.75	38.28
15H-5	150	134.89	37.60
16H-5	150	144.39	41.14
17H-3	150	150.89	36.76
17H-5	150	153.89	36.26
18H-3	150	160.39	39.25
18H-5	150	163.39	39.78
19H-3	136	169.75	35.42
19H-5	137	172.76	28.09
20H-3	136	179.25	33.64
20H-5	136	182.25	33.84
23H-3	136	191.04	34.67
23H-5	136	194.04	37.69
24H-3	136	200.54	36.87
24H-5	136	203.54	90.40
25H-3	136	210.04	157.08
25H-5	136	213.04	93.61
26H-3	136	219.55	45.63
26H-5	136	222.55	314.16
27H-3	137	229.06	314.16
28H-3	136	238.55	314.16

4.3 *Proboscia curvirostris* and *Proboscia barboi*

4.3.1 Identification

Identification of these species was based on the presence or absence of the dorsal fin. Heavily dissolved frustules but with distinguishable remains of the dorsal fin and intermediate specimens between *P. barboi* and *P. curvirostris* with a dorsal fin were counted as *P. curviostris*.

4.3.2 Measurements

In order to study the intermediate specimens of *P. barboi* and *P. curvirostris*, 13 specimens from sample 11H-CC and 14H-3 respectively, were measured as well as 13 specimens considered to be intermediate, from sample 24H-5. The samples were selected for containing fairly well preserved and morphologically average specimens of *P. barboi* and *P. curvirostris*, suitable for the measurements. Although a larger sampling would be necessary to make a rigorous morphometric study, this number of specimens allows to have a reference point to which the intermediate specimens can be compared, which was the main purpose.

Apart from the dorsal fin, two main features were used to distinguish the *P. curvirostris* and *P. barboi*: the width and curvature of the tube. The width (µm) was measured at the region between the maximum curvature and the tip of the tube (fig. 4.3), closer to the former, as the tube in some specimens appears to become narrower towards the apex. The curvature of the tube was measured on the ventral side. The employed method consisted in drawing two straight lines (on the ventral side), one parallel to the direction of the tube's distal end and another parallel to its more proximal part and afterwards measuring the angle of the two lines (fig. 4.4).

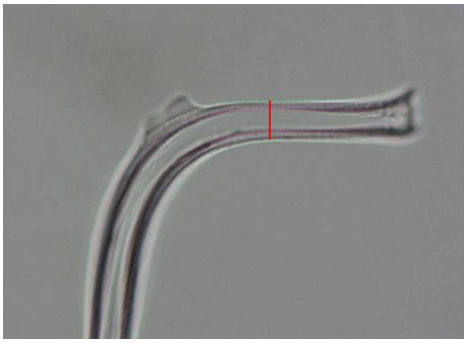

Figure 4.3 - Measurement of the tube's width.

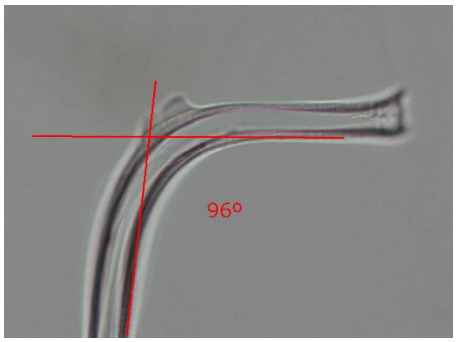

Figure 4.4 - Measurement of the tube's curvature.

4.4 Thalassiosira jouseae

4.4.1.1 Identification

Identification was based on Akiba (1986) and the identification of *T. nidulus* relied on Akiba (1986) and SEM imaging of Koç and Scherer (1996). A few *T. nidulus* valves were included under *T. jouseae* during the counting process, although not in a sufficient number that would undermine the counts.

4.4.1.2 Description

The description of *T. jouseae* was made based on a sizeable number of specimens more than a hundred, from samples U1340A-4H-CC (32.56 Mid CSF m) to 40H-1 (343.28 Mid CSF m) which corresponds to a 2.13-0.26 Ma time interval in the Pleistocene Epoch. It is merely a qualitative description of *T. jouseae* with the purpose of complementing the original description by Akiba (1986). Likewise, *T. nidulus* was also described based on a few specimens from samples U1340A-20H-3, 19H-5, 9H-5, 9H-3 and 8H-3, where this species was identified.

4.5 Paleoecology – used counts and data

In the paleoecology subchapter, the relative abundance and productivity graphics were constructed using the counts and data of Stroynowski et al. (2015) and thus the interpretation of *P. curvirostris*, *P. barboi* and *T. jouseae* abundance records is based on said publication. The counts of *P. barboi* on samples U1340A-18H-3, 18H-5, 19H-3 and the counts of *P. curvirostris* on sample U1340A-25H-5 are not considered, as in the counting process of this study the referred species were not identified on said samples (fig. 5.1).

4.6 Environmental proxies

The environmental proxies used in this study are summarized in the following table.

Table 4.2 - List of the environmental proxies according to Sancetta (1982) and von Quillfeldt (2000, 2001).

Proxy group	**Species**	**Environmental factor**
Neodenticula spp.	*Neodenticula kamtschatika, Neodenticula koizumii and Neodenticula seminae*	Alaskan Stream
Sea ice species	*Thalassiosira gravida, Thalassiosira antiqua, Thalassiosira nordenskioeldii, Thalassiosira hyalina, Stellarima microtrias, Porosira glacialis, Paralia sol, Paralia sulcata, Nitzschia sp., Fossula arctica, Fragilariopsis curta, Fragilariopsis cylindrus*	Presence or influence of sea ice (e.g. iceberg transportation)
Chaetoceros spp.	-	Productivity
Mat-forming shade flora species	*Rhizosolenia hebetata f. hebetata, Rhizosolenia hebetata f. hiemalis, Rhizosolenia hebetata f. seminspina, Rhizosolenia stylisformis, Coscinodiscus marginatus*	water stratification
Rhizosolenia spp.	*Rhizosolenia hebetata f. hebetata, Rhizosolenia hebetata f. hiemalis, Rhizosolenia hebetata f. seminspina, Rhizosolenia stylisformis.*	water stratification

5 Results and Discussion

5.1 Biostratigraphy

At U1340, the LO of *P. curvirostris*, *T. jouseae* and *P. barboi* occur at 0.33-0.26 Ma (sample U1340A-5H-CC), at 0.26-0.23 Ma (sample U1340A-4H-CC) and at 1.39-1.37 Ma sample 24H-5, respectively (table 5.1; fig. 5.1b). In samples up-core from the observed LO of *P. barboi* at sample U1340A-24H-5, no *P. barboi* valves were found except for samples 23H-3 (191.04 m; one valve), 11H-CC (99.17 m; 21 valves) and 4H-CC (32.56 m; 1 valve). Specimens of *P. barboi* in sample 11H-CC were well preserved, while *P. curvirostris* is absent which may indicate that these events in the same sample are not a mere coincidence and not a result of reworking. Hence, an alternative LO for *P. barboi* could be set at 0.67-0.65 Ma (sample U1340A-11H-CC, 99.17 m), which is also approximately the same age when this species disappears at Site U1343. However, the LO of *P. barboi* was set at sample 24H-5 due to the great scarcity of occurrences after this sample. On the other hand, in Takahashi et al. (2011b) the LOs of these species both occur at 0.3 Ma (sample U1340A-5H-CC). The previously established LOs of these species in core U1340A are all set at 0.3 Ma (Takahashi et al., 2011b) differing on the LOs of *T. jouseae* and *P. barboi*.

Table 5.1 - Datums of *P. curvirotris*, *P. barboi* and *T. jouseae* of core U1340A (this work).

		Age (Ma)	Sample	Depth (mid CSF m)	#valves counted
P. curvirostris	LO	0.33-0.26	U1340A-5H-CC	42.13	94
	FO	1.52-1.56	U1340A-26H-5	222.55	1
	FCO	1.44-1.39	U1340A-24H-5	203.54	60
P. barboi	LO	1.39-1.37	U1340A-24H-5	203.54	4
	LCO	1.44-1.39	U1340A-25H-3	210.04	30
T. jouseae	LO	0.26-0.23	U1340A-4H-CC	32.56	4
	LCO	0.38-0.33	U1340A-6H-CC	51.68	51

An important observation in core U1340A is that the occurrences of *P. barboi* and *P. curvirostris* do not overlap and are mutually exclusive, that is, both species virtually never occur in the same sample. In sample 11H-CC, when there is an abundance spike of *P. barboi*, *P. curvirostris* becomes abruptly absent. In the few samples where both species co-occur (samples 23H-3 and 24H-5) the quantity of one of the species is negligible and the specimens found are dubious.

The counts performed in this study match well those of Stroynowski et al. (2015) despite the lower values of productivity which might be due to the higher area observed (fig. 5.1). Nevertheless, at approximately 160 m depth (mid CSF), a few valves of *P. barboi* were found (samples U1340A-18H-3, 18H-5, 19H-3) and some valves of *P. curvirostris* were counted around

213 m depth mid CSF (sample U1340A-25H-5; Stroynowski et al., 2015) which were not observed during the counts of this study.

5.2 Paleoecology

Note: the following discussion of the paleoecology of the studied species is made in reference to fig. 5.6 unless otherwise indicated.

5.2.1 Proboscia barboi

P. barboi appears at 2.7 Ma, when the first signs of sea ice diatoms subtly increase at Bowers Ridge (Site U1340) and also coinciding with the inception of Northern Hemisphere Glaciation (NHG; Takahashi et al., 2011; Maslin et al., 1996). At this time in the Bering Sea, diatom biodiversity and productivity increased with a marked change in the diatom assemblage, indicating enhanced seasonality and stratification (Stroynowski et al., 2015). Fluctuations of relative abundances (RA) of *P. barboi* show an increasing trend starting from 2.1 Ma, coinciding with a long term progressive increase of sea ice assemblages in Site U1340, up to 10%-20% of the total respective assemblage (Takahashi et al., 2011). From 2 to 1.2 Ma, the Bering Sea is characterized by stratified and nutrient-depleted summer waters as indicated by the absence and reduced presence of the high-productivity indicators *Chaetoceros* (resting and vegetative spores) and *Thalassiothrix longissima* (Stroynowski et al., 2015). The authors suggest that the most likely cause of stratification is by ice melt. *Rhizosolenia spp.* (*R. hebetata f. hebetata*; *R. hebetata f. hemialis*; *R. hebetata f. semispina* and *R. styliformis*), which are shade flora species, also began to appear with more frequency after 2.0 Ma (Stroynowski et al., 2015), and their RA fluctuations show good correlation with *P. barboi* (fig. 5.3). The fairly coincident rise and positive correlation of *Rhizosolenia spp.* and *P. barboi*, together with the positive responses to sea ice influence and resultant water stratification, support the notion of *P. barboi* being a shade flora species that proliferated colder waters.

P. barboi disappears from Site U1340 geological record at 1.4 Ma, being replaced at the same time by *P. curvirostris*, despite the curious isolated abundance spike of *P. barboi* resurfacing at 0.7 Ma (sample 11H-CC). The RA of *P. barboi* generally do not exceed 8% across its stratigraphic span and have a mean value of 1.6 % (fig. 5.4; table 5.2).

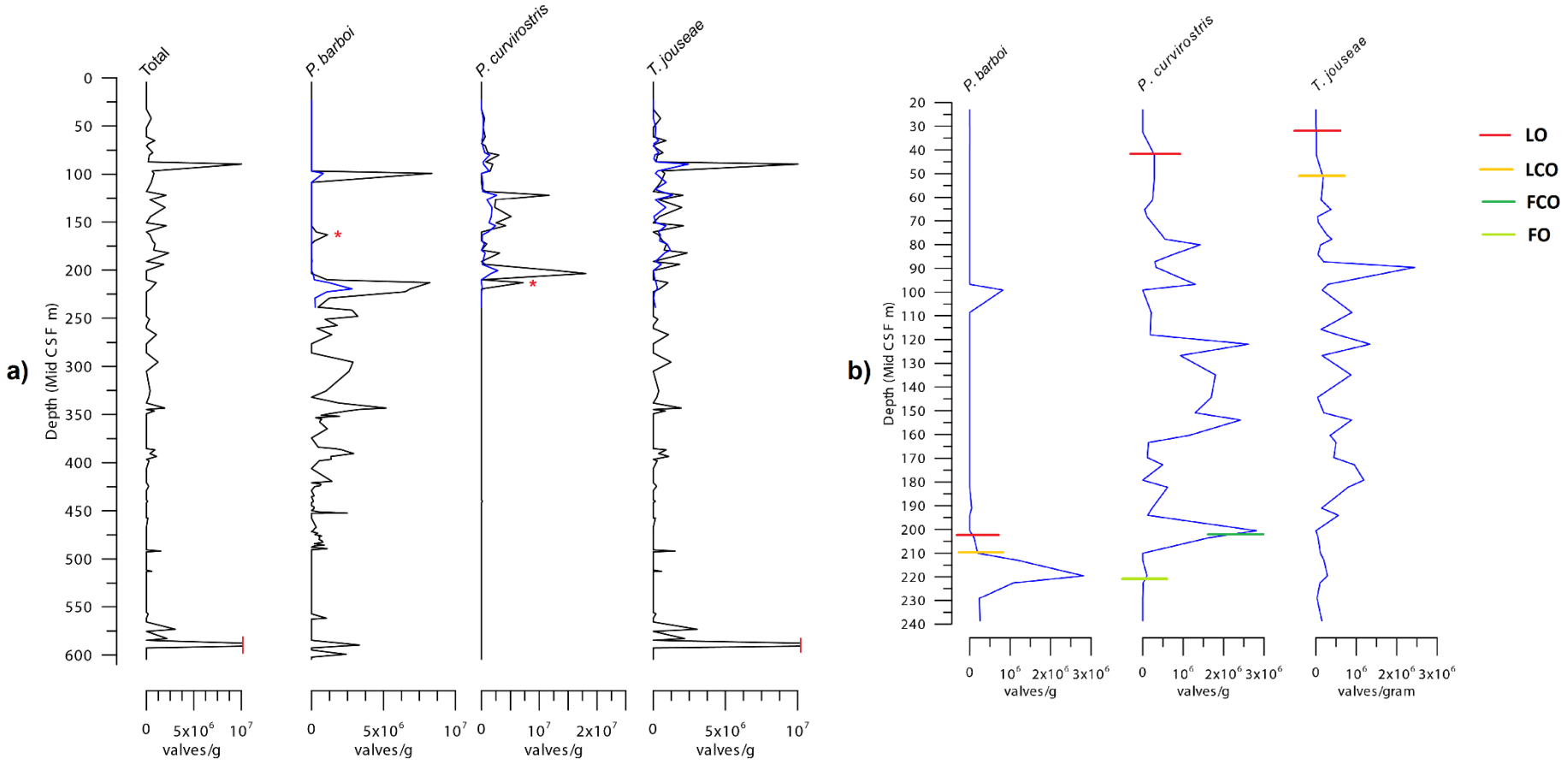

Figure 5.1 - a) Productivity of *Proboscia barboi*, *P. curvirostris* and *Thalassiosira jouseae* plotted with depth (blue, this work) superimposed with the productivity of Stroynowski, 2015; Values higher than 10^7 valves/g were clipped off. b) Productivity and biostratigraphic events of the same species (this work). Red asterisk: peaks not considered.

As discussed above, the LO's of *P. barboi* vary depending on location and may be divided into two groups: sites where both the LO of *P. barboi* and *P. curvirostris* co-occur, and sites where the LO of *P. barboi* occur around the same time as the FO of *P. curvirostris*. At Site U1340, the LO of *P. barboi* belongs to the latter group as *P. barboi* disappears at 1.4 Ma where the FO of *P. curvirostris* is established. Whereas at Site U1341, *P. barboi* disappeared at 0.42-0.47 Ma (Onodera et al., 2013), although its RA somewhat decreases after the FO of *P. curvirostris*. Hence, at two close locations, one on the western flank and the other on the south-eastern part of the Bowers Ridge, *P. barboi* disappears at different ages, which suggest differences in the environmental conditions affecting *P. barboi*. However, at Site 188 (Koizumi, 1973) which is in the vicinity of Site U1341 (fig. 1.4), the LO of *P. barboi* does not match that of the latter Site, as it occurs near the FO of *P. curvirostris* and therefore the stratigraphic range of *P. barboi* in this region should be further investigated.

5.2.2 Proboscia curvirostris

P. curvirostris appearance around 1.4 Ma is marked by a large peak of 14% RA and coincides with a peak of AS marker species *Neodenticula* spp. (56 %) and a drop in sea ice species (1%), which indicates that its appearance occurred in a relatively warm period under relatively high influence of AS waters. It is also not a particularly nutrient-abundant period with frequent upwelling as can be observed by the low abundance of *Chaetoceros spp.* Furthermore, the FCO of *P. curvirostris* is the largest RA peak which indicates that the environmental conditions referred above were favourable or at least tolerable when *P. curvirostris* appeared.

The abundance record shows a general tendency for a progressive decline in the amplitude of peaks of *P. curvirostris* which may be a reflection of the progressive intensification of the NHG. However, in neighbouring Site U1341, an opposite trend, with an increase of the RA peaks is observed (fig. 5.2). The first peak occurs at 150 m depth with 8 % RA, followed by another peak of 10 % at 97 m depth, and lastly a peak of 16 % at 70 m depth. As discussed above, during the past 270 kyr, the western and eastern sides of the Bowers Ridge faced different influence of AS waters and consequently sea ice as the eastern Aleutian passes (e.g. Amchitka Pass), were more restricted during glacial periods (Katsuki and Takahashi, 2005). Extending this reasoning to an earlier time interval, it is possible that the opposite trends in RA of *P. curvirostris* at sites U1340 (eastern side of Bowers Ridge) and U1341 (western side) were due to a higher influence of AS waters in the western side of the Bowers Ridge mitigating the effects of the NHG and allowing higher abundances of *P. curvirostris* in the western side of the Bowers Ridge compared to the eastern side.

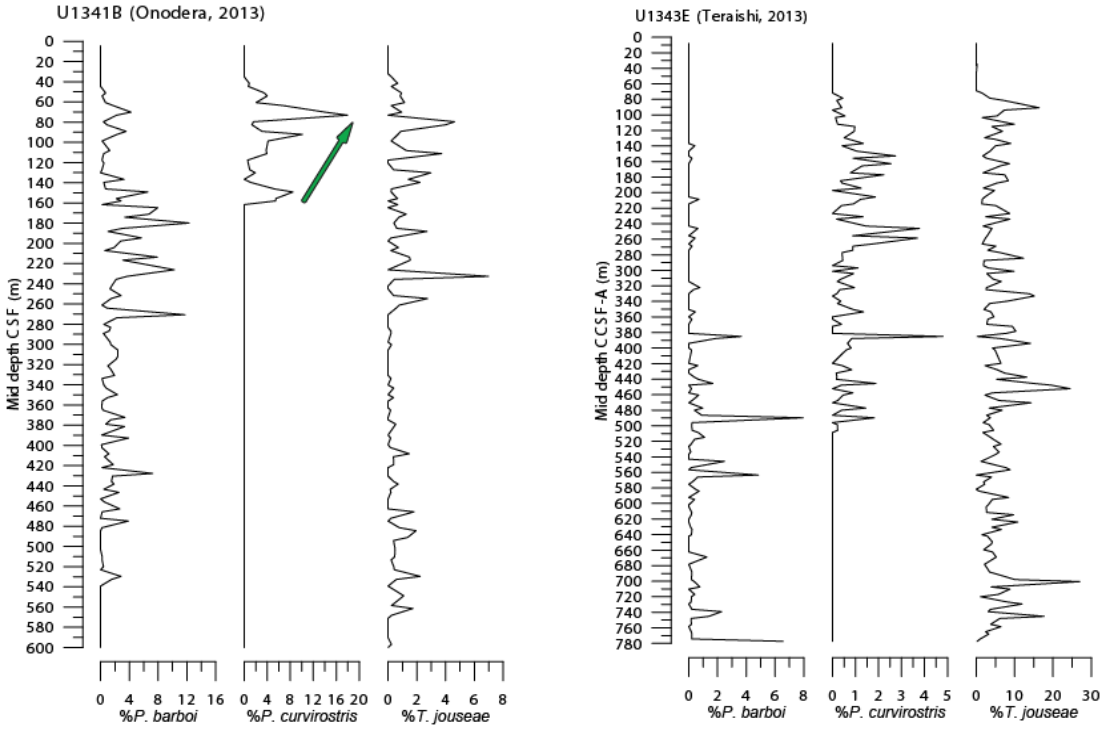

Figure 5.2 - RA of *P. barboi*, *P. curvirostris* and *T. jouseae* in cores U1341B and U1343E. Green arrow denotes the increase in RA of *P. curvirostris*. Plots constructed with the supplementary data of Onodera et al. (2013) and Teraishi et al. (2013); *Chaetoceros* considered.

The sudden absence of *P. curvirostris* at ~0.7 coincides well with a big 40% drop of *N. seminae* (from 50% to 7% RA), a large peak of sea ice species (31%) and a peak of *Chaetoceros spp.* (17%) which indicate a cold period with enhanced sea ice influence and somewhat nutrient rich waters. The RA of other mat-forming shade flora (MFSF) species also drops. The combination of these environmental factors, especially the cold/sea ice factor may well be the cause for the short absence of *P. curvirostris*. Curiously at the same time, *P. barboi* unexpectedly resurfaces. The absence of *P. curvirostris* was registered in 2 consecutive samples (U1340A-12H-CC, 108.61 mid CSF m; 11H-CC, 99.17 Mid CSF m) while *P. barboi* re-appears in a single sample (11H-CC).

The LO of *P. curvirostris* occurs at 0.3 Ma, in agreement with the other North Pacific sites. Close to the extinction of *P. curvirostris*, the *Rhizosolenia* MFSF group (mostly comprised of *R. hebetata f. hebetata*) shows a significant increase up to 27% (fig. 5.3), equivalent to its rise in the Subarctic, where Sancetta and Silvestri (1984) suggested that *R. hebetata* "ecologically replaces" *P. curvirostris* and suggested that the intensification of glacial conditions wiped out *P. curvirostris* and created a new or expanded niche which allowed *R. hebetata* to flourish.

The RA of *P. curvirostris* and *P. barboi* at Site U1341 are comparatively similar to Site U1340, while northward at the Bering Slope Site U1343 they are significantly lower (fig. 5.4).

Mean values of RAs of *P. barboi* and *P. curvirostris* at Site U1340 are about 4 times higher than at Site U1343 (fig. 5.4; table 5.2). The low abundances of *P. curvirostris* and *P. barboi* at Site U1343 suggest that they do not have a particular preference for the upwelling regimes or sea ice influence of the Bering Slope and fits into the likely shade flora ecology of *P. curvirostris* and *P. barboi*, since *Proboscia* in high latitudes are generally not associated with upwelling or part of the sea ice community (Takahashi et al., 1994).

At the Southern Bering Sea sites as well as the North Subarctic Pacific where the Alaskan Current is the dominant water current (Leg 19 DSDP), RA of both *Proboscia* species vary between 0.5% and 2.5% and less often between 3% and 9.5% in a 200 total valve count (*Chaetoceros* not counted; Koizumi, 1973). Their low abundance in the Alaskan Stream domain requires further investigation, however it does suggest an ecological preference for colder, less saline waters.

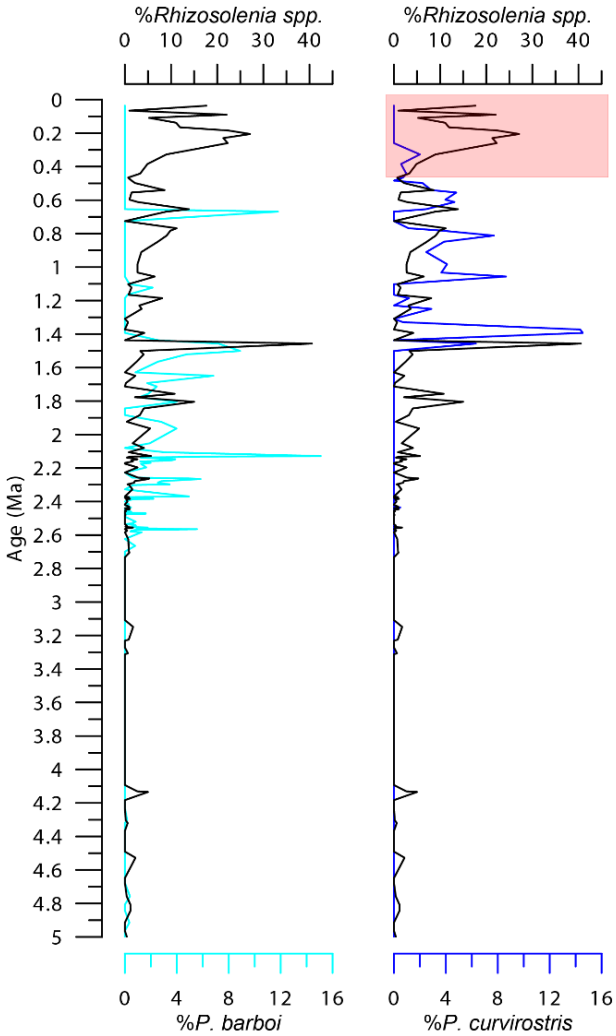

Figure 5.3 - RA of *P. barboi* and *P. curvirostris* compared with RA of *Rhizosolenia* spp. Red area denotes the rise of *Rhizosolenia* spp. (mainly *R. hebetata*).

5.2.3 Thalassiosira jouseae

Subtle occurrences of *T. jouseae* started at around 2.5 Ma, and can be considered part of the diatom assemblage reorganization and enhanced productivity that began circa. 2.7 Ma, coinciding with the onset of NHG (Stroynowski et al., 2015). With the exception of the sudden abundance spike at 0.65 Ma (24.3% at sample 10H-CC), the RA of *T. jouseae* remained low and at relatively stable fluctuations below 4% with no apparent long term trend which shows that *T. jouseae* over the long term, did not respond to the progressive trend of seasonally stratified waters (Stroynowski et al., 2015), nor the development of glacial/interglacial cycles. Hence, water stratification does not seem to be a very important part of the ecology of *T. jouseae*. Strong negative correlation with *Neodenticula* spp. also supports a preference for colder waters and positive response to cold periods.

The RA of *T. jouseae* are similar to neighbouring Bowers Ridge Site U1341, but not at Site U1343, where its RAs are considerably higher, with mean values of 5.5%, more than five times than in the Bowers Ridge Sites (fig. 5.4; table 5.2). The Bering Slope region is part of the Green Belt and therefore characterized for high productivity, regular upwelling regimes and by annual fluctuations in sea-ice cover (the extent of which also vary on the glacial and interglacial time scale) so the high abundances of *T. jouseae* in the Bering Slope strongly suggest that this species was well adapted to upwelling regimes and/or sea ice of the Bering Slope and has a neritic distribution. Comparison with the RA and productivity record (fig. 5.5) of the sea ice group shows no clear correlation, that is, there is no consistent correlation pattern throughout the abundance record. On the other hand comparison with the RA and productivity of *Chaetoceros spp*. generally shows positive correlation which indicates a preference for neritic and nutrient rich waters. Whether, *T. jouseae* may be related to sea ice is not conclusive but since the Bering Slope is affected by sea ice cover, it is plausible that, together with upwelling, sea ice is part of the ecology of *T. jouseae*.

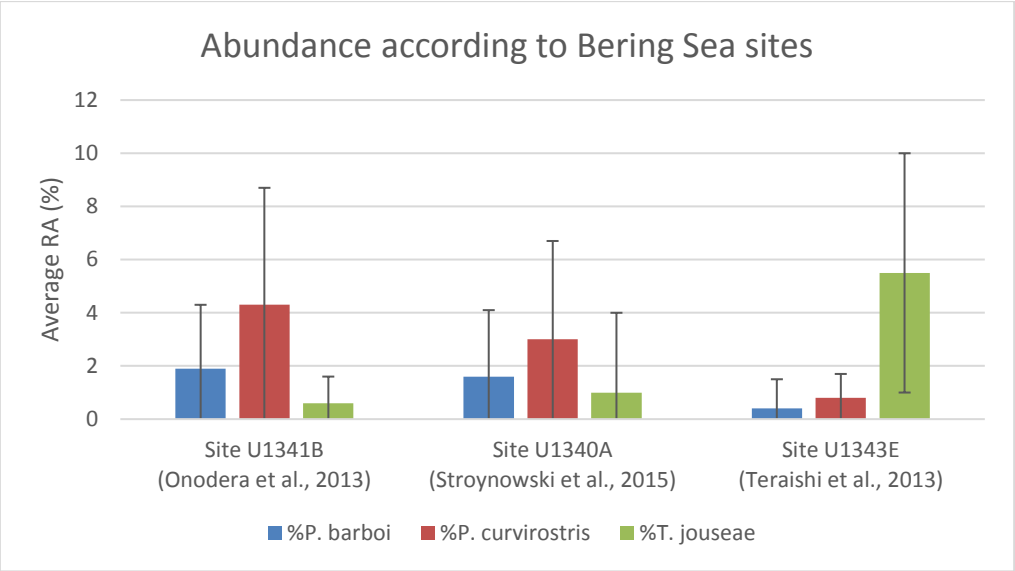

Figure 5.4 - Average RA of *P. barboi*, *P. curvirostris* and *T. jouseae* at Sites U1341, U1340 and U1343; *Chaetoceros* considered.

Table 5.2 - Mean percentages and range of RA of *P. barboi*, *P. curvirostris* and *T. jouseae* of coresU1341B, U1340A and U1343E. The depth interval considered for the calculations is also shown. *Chaetoceros* considered.

		Core U1341B (Onodera et al., 2013)	Core U1340A (Stroynowski et al., 2015)	Core U1343E (Teraishi et al., 2013)
%P. barboi	Average	1.9	1.6	0.4
	Range (min. – max.)	0-12.3	0 - 15.1	0 - 8.0
	depth interval (m)	51.15-532.65	99.17-489.27	139.73-777.34
%P. curvirostris	Average	4.3	3	0.8
	Range (min. – max.)	[0 - 18.0]	[0 - 14.6]	0 - 4.8
	depth interval (m)	41.64-157.99	42.13-213.04	81.45-505.79
%T. jouseae	Average	0.6	1	5.5
	Range (min. – max.)	0 - 7.0	0 -24.3	0-27.0
	depth interval (m)	35.15-599.95	42.13-424.93	71.74-777.34

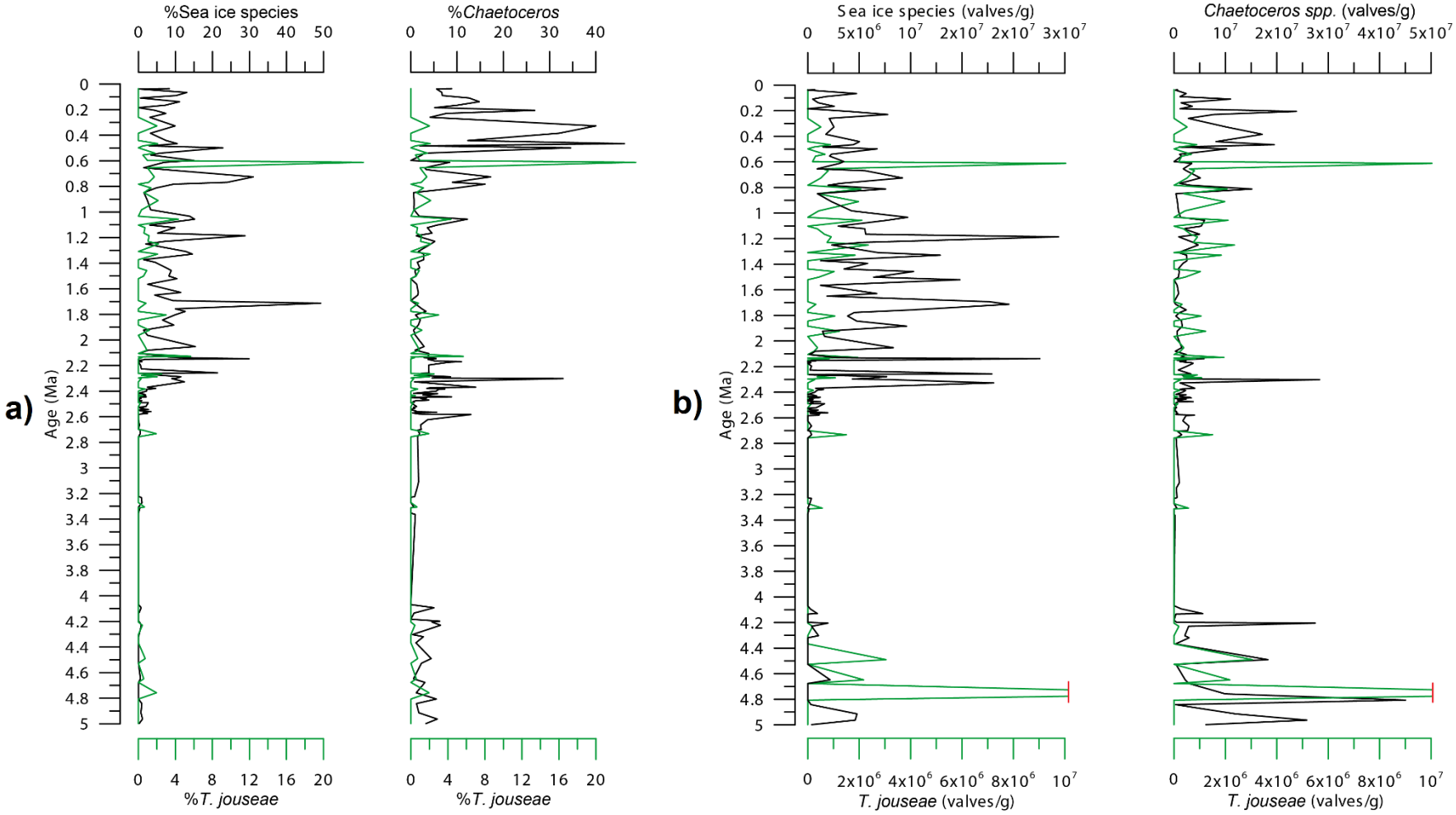

Figure 5.5 – *T. jouseae* compared with the sea ice species and *Chaetoceros* sp. records in RA (a) and productivity (b). Values above 10^7 were clipped off.

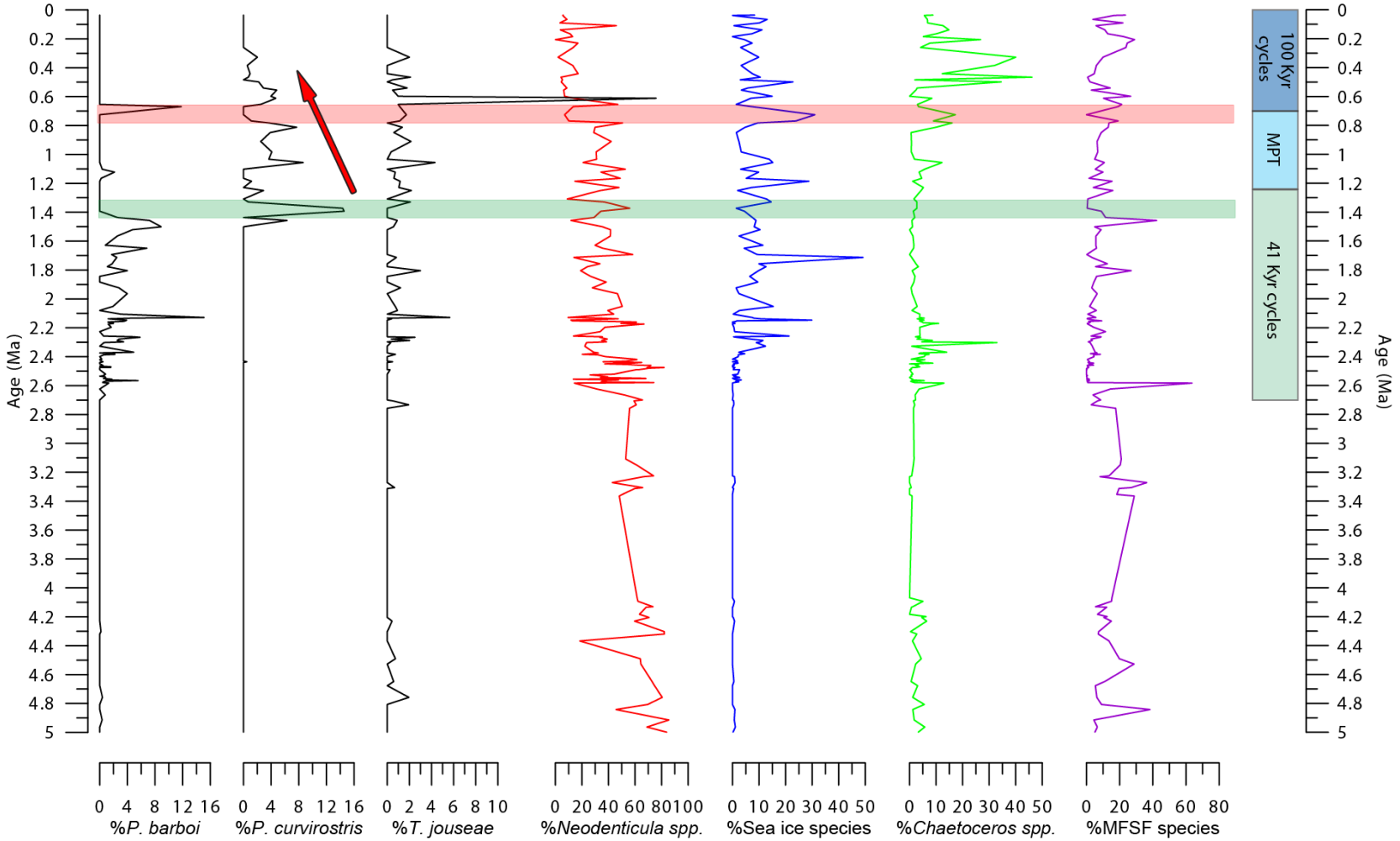

Figure 5.6 - RA of *P. barboi*, *P. curvirostris* and *T. jouseae* juxtaposed with selected environmental proxies. The green bar marks the FCO of *P. curvirostris* and the LO of *P. barboi*. Red bar marks the sudden disappearance and resurface of *P. curvirostris* and *P. barboi*, respectively. Red arrow denotes the progressive decrease in RA of *P. curvirostris*. MPT – Mid Pleistocene Transition.

5.3 Morphology

5.3.1 Intermediate specimens of *Proboscia*

P. curvirostris generally has a lower tube width and a lower curvature angle than *P. barboi* (Akiba and Yanagisawa, 1986). The measurements also show this morphometric difference (table 5.3; pl. 1, figs. 1, 2, 3, 4).

Table 5.3 - Measurements of specimens of *P. curvirostris* (SpC) and *P. barboi* (SpB).

P. curvirostris			*P. barboi*		
SpC	width (µm)	curvature (°)	**SpB**	width (µm)	curvature (°)
1	6.7	97	**1**	12.0	114
2	8.9	104	**2**	14.2	115
3	7.0	133	**3**	9.3	112
4	9.3	105	**4**	11.1	104
5	9.3	100	**5**	9.3	132
6	7.4	120	**6**	11.1	124
7	7.7	98	**7**	9.3	123
8	7.4	103	**8**	13.0	117
9	8.5	125	**9**	13.0	119
10	8.1	97	**10**	12.3	116
11	9.3	110	**11**	8.0	111
12	6.7	114	**12**	13.0	121
13	10.0	93	**13**	13.0	108
Mean	8.2	107.6	**Mean**	11.4	117

A number of intermediate specimens were found on sample U1340A-24H-5, on which the FCO of *P. curvirostris* and LO of *P. barboi* occur. The specimens (table 5.4; pl. 1 and 2) were considered intermediate for being bigger and bulkier than the average *P. curvirostris*, often the same size as *P. barboi* (e.g. pl. 1, fig. 5; pl. 2, fig. 3), or/and bearing an unusual dorsal fin, lower and longer (pl. 2, figs. 1, 4), “over developed” (pl. 2, fig. 2) or “under developed” (pl. 1, fig. 5; pl. 2, figs. 5, 6), sometimes reduced to a small “bump” (pl. 2, fig. 6). Also, whereas the dorsal fin of *P. curvirostris* points toward the tip of the tube, in these intermediate specimens the dorsal fin is often not oriented (pl. 2, figs. 1, 5). It could be argued that these shapes are simply the result of bad preservation and dissolution of the dorsal fin but since the specimens were well preserved and were relatively recurrent on sample U1340A-24H-5, it is likely not the case.

The fact that these intermediate specimens occur on the sample of the LO of *P. barboi* and FCO of *P. curvirostris* also suggests that said specimens are the evidence of the evolutionary transition from *P. barboi* to *P. curvirostris*.

Table 5.4 - Measurements of intermediate specimens (SpI).

Intermediate specimens		
SpI	width (µm)	curvature (°)
1	9.3	98
2	11.7	106
3	12.3	114
4	9.9	96
5	10.5	103
6	11.7	109
7	8.6	111
8	8.0	91
9	8.6	89
10	8.6	86
11	8.0	100
12	11.1	97
13	9.3	84
Mean	9.8	98.8

5.3.2 Description of *Thalassiosira jouseae* and *Thalassiosira nidulus*

5.3.2.1 Thalassiosira jouseae

The size of *T. jouseae* varies between 9-31 µm. The areolae are generally distributed sparsely on the valve face, sometimes relatively uniformly (plate 3, figs. 1, 2, 7). Bigger valves (> 15 µm), often display a pattern of radial and sub-radial rows (pl. 4, fig. 1). The areolation often seems to be confined to a central area or disc, leaving the outermost periphery of the valve face hyaline (pl. 3, figs. 1, 2, 5, 7; pl. 4, fig 1), although some exceptions occur where areolation covers the valve face till the very base of the sub-marginal spines (pl. 3, figs. 3, 4; pl. 4, figs. 5, 6). The valve face is usually convex, to varying extents. These features are best observed in more preserved and silicified valves (pl. 3, figs. 1, 2, 3, 4, 7, 8; pl. 4, fig. 1), which were often encountered and really stand out in relation to the other *T. jouseae* valves. The less preserved valves (which have a grainy or coarse appearance) tend to display areolae arranged more closely together (pl. 3, figs. 5, 6), often tightly close (pl. 4, figs. 5, 6). The arrangement is often in radial and sub-radial rows or more aptly termed, concentric rows (pl. 4, figs. 5, 6). Like the more silicified type, the periphery of the valve face can be mostly free of areolation but more often is the areolation covering the whole valve face. In some of these valves, it is possible to observe the areolae arrangement of the holotype specimen (pl. 3, fig. 5) which seems like a central "aggregate" of areolae.

The sub-marginal spines of highly silicified valves are conspicuous and long, and it is easy to discern the connection between the basal parts of each spine, which gives the characteristic

appearance of a crown (pl. 3, figs. 4, 8; pl. 4, figs. 1). In other valves, the spines are much shorter and the basal parts are not as distinctively united (pl. 3, figs. 5, 6; pl. 4, figs. 5, 6).

The margin is striated and slanting relative to the valve face. It is formed by several ribs projecting from the girdle, outward to a circular marginal rim (pl. 4, figs. 2, 3, 4). While, more silicified valves have a clear marginal rim, in other valves this structure is thinner and sometimes poorly discernible.

The observations showed that the morphology of *T. jouseae* is considerably variable regarding the areolation and the sub-marginal spines. Two main morphological types can be recognized:

- Type I; usually sparse areolae which in bigger valves tend to be arranged in the radial and sub-radial rows pattern, conspicuous medium to long sub-marginal spines and united bases of the spines easily discernible. This type is highly silicified and distinct when observed at LM.
- Type II; more common; areolae arranged more closely together, small sub-marginal spines and basal parts not so distinctly united. The marginal rim is sometimes poorly discernible. The areolation of the holotype specimen can be often recognized in type II. The valves have a coarser appearance due to lower silicification and preservation.

Naturally, at the LM one can come across many intermediates between the two types but nonetheless, any given *T. jouseae* valve can be attributed to one of them (unless it is some morphologic variation).

5.3.2.2 Thalassiosira nidulus

T. nidulus is within the size range of *T. jouseae*. It is densely areolated, with areolae covering all the valve face, from the centre to the base of the sub-marginal spines in concentric rows. None of the specimens observed displayed the areolation restricted to the central area of the valve face, as often happens in *T. jouseae*. The valve face is usually mostly flat. The sub-marginal spines look in fact separate from each other as had already been noted (Akiba, 1986). However, this can also be said of many valves of *T. jouseae* type II. In addition, the spines seem to have a different shape when compared to *T. jouseae* looking triangle-shaped and less tapering (pl. 4, fig. 7; fig. 5.7), although this needs further investigation. The marginal rim is usually absent or poorly discernible (pl. 4, fig. 8). Although valves of *T. jouseae* type II (pl. 4; figs. 5, 6) are often quite ambiguously similar to *T. nidulus*, the latter species still has a distinct overall appearance (pl. 4, fig. 7). Thus, the most relevant differences of *T. nidulus* in relation to *T. jouseae* are the

dense areolation covering all of the valve face, the triangle-shaped separate sub-marginal spines, and more secondarily the absence or not easily discernible marginal rim (pl. 4, figs. 7, 8).

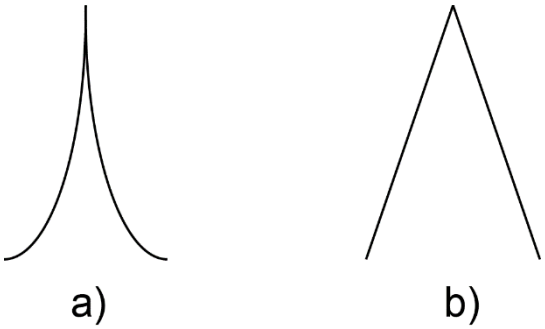

Figure 5.7 - Suggested shapes of the sub-marginal spines of *T. jouseae* (best observed in type I; a) and *T. nidulus* (b).

6 Conclusions

- The LOs of *P. curvirostris*, *T. jouseae* and *P. barboi* at Site U1340 were identified at 0.33-0.26 Ma, 0.26-0.23 Ma, and 1.39-1.37 Ma, respectively.
- *Proboscia barboi* and *P. curvirostris* do not co-occur in the stratigraphic record of core U1340A.
- The very low abundance of *P. barboi* and *P. curvirostris* at Site U1343, located in the Bering Slope, a region characterized by regular upwelling and sea ice influence, suggests that this species is not adapted to these environments and fits into its assumed preference for water stratification.
- The significantly higher abundance of *Thalassiosira jouseae* at Site U1343 (Bering Slope), compared to Sites U1340 and U1341 (Bowers Ridge) suggests that *T. jouseae* is a neritic species adapted to high productivity waters and upwelling regimes. The positive correlation of the RAs of *T. jouseae* and *Chaetoceros* spp. (Site U1340) also supports this hypothesis. Furthermore, being the Bering Slope region a region of high sea ice influence it is plausible that *T. jouseae* may have been adapted to sea ice although correlation of its RA with that of the sea ice group was inconclusive.
- Intermediate specimens between *P. barboi* and *P. curvirostris* were found and are characterized for having sizes comparable to *P. barboi* and a dorsal fin, often smaller and/or with atypical shapes.
- *T. jouseae* was described and two morphological types characterized based on the areolation, sub-marginal spines and marginal rim.
- *T. nidulus* was described and can be distinguished from *T. jouseae* by its dense areolation covering all of the valve face, the triangle-shaped separate sub-marginal spines, and more secondarily the absence or not easily discernible marginal rim.

7 References

Abrantes, F., Gil, I., Lopes, C. and Castro, M., 2005. Quantitative diatom analyses—a faster cleaning procedure. *Deep Sea Research Part I: Oceanographic Research Papers*, *52*(1), pp. 189-198.

Abrantes, F. and Gil, I.M., 2007. Marine diatoms. *Encyclopedia of Quaternary Sciences: Amsterdam, Elsevier*, pp. 1668-1678.

Akiba, F., 1986. Middle Miocene to Quaternary diatom biostratigraphy in the Nankai Trough and Japan Trench, and modified Lower Miocene through Quaternary diatom zones for middle-to-high latitudes of the North Pacific. *Initial reports of the deep sea drilling project, 87*, pp. 393-480.

Akiba, F. and Yanagisawa, Y., 1986. Taxonomy, morphology and phylogeny of the Neogene diatom zonal marker species in the middle-to-high latitudes of the North Pacific. *Init. Rep. DSDP, 87*, pp. 483-554.

Alexander, V. and Niebauer, H.J., 1981. Oceanography of the eastern Bering Sea ice-edge zone in spring. *Limnol. Oceanogr., 26*(6), pp. 1111-1125.

Armstrong, H.A. and Brasier, M.D., 2013. *Microfossils*. 2nd ed. Blackwell Publishing, Oxford, UK, pp. 296.

Barron, J.A., 1980. Lower Miocene to Quaternary diatom biostratigraphy of Leg 57, off Northeastern Japan, Deep Sea Drilling Project. *Scientific Party, Init. Repts. DSDP, 56, 57, Pt. 2: Washington (U.S. Govt. Printing Office)*, 641-685.

Barron, J., 1985. Late Eocene to Holocene diatom biostratigraphy of the equatorial Pacific Ocean, Deep Sea Drilling Project Leg 85. *Initial Reports of the Deep Sea Drilling Project. US Government Printing Office, Washington, 85* (OCT), pp. 413–456.

Barron, J.A. and Gladenkov, A.Y., 1995. Early Miocene to Pleistocene diatom stratigraphy of Leg 145. *Proceedings of the Ocean Drilling Program, Scientific Results, 145*, pp. 3-19.

Brun, J., 1894. Espèces nouvelles. *Le Diatomiste*, *2*(16), pp. 72-78, 86-88.

Brun, J. and Tempère, J.A., 1889. Diatomées fossiles du Japon: Espèces marines and nouvelles des calcaires argileux de Sendaï and Yedo. *Société de physique et d'histoire naturelle de Genève, 30*(9), pp. 1-75.

Caisse, B.A., 2012. Diatoms as Recorders of Sea Ice in the Bering and Chukchi Seas : Proxy Development and Application. PhD thesis. University of Massachusetts-Amherst, pp. 190.

Donahue, J.G., 1970. Pleistocene diatoms as climatic indicators in North Pacific sediments. *Geological Society of America Memoirs, 126*, pp. 121-138.

Glezer, S. I., Makarova, I. V. (editor -in-chief), Moisseeva, A. I. and Nikolaev, V. A. 1988. The diatoms of the USSR, Fossil and Recent: Pyxidiculaceae, Thalassiosiropsidaceae, Triceratiaceae, Thalassiosiraceae. *NAUKA 2*(1), pp. 116.

Gordon, R. and Seckbach, J. eds., 2012. *The science of Algal fuels: phycology, geology, biophotonics, genomics and nanotechnology* (Vol. 25). Springer, Science and Business media. Dordrecht, Netherlands.

Gran, H.H., 1900. Bemerkungen über einige Planktondiatomeen. *Nyt Magazin for Naturvidenskaberne (Kristiania), 38*, pp. 103-126.

Hajós, M., 1976. Upper Eocene and Lower Oligocene Diatomaceae, Archaeomonadaceae, and Silicoflagellate in Southwestern Pacific Sediments, DSDP Leg 29. *Initial Reports of the Deep Sea Drilling Project, 35*, pp. 817-883.

Hargraves, P.E., 1986. The relationship of some fossil diatom genera to resting spores. *Proceedings of the Eighth International Diatom Symposium. O. Koeltz, Koenigstein*. pp. 67-80.

Hasle, G.R., Syvertsen, E.E., Steidinger, K.A., Tangen, K. and Tomas, C.R., 1996. *Identifying marine diatoms and dinoflagellates*. Academic Press, pp. 598.

Hernández-Becerril, D.U., 1995. Planktonic diatoms from the Gulf of California and coasts off Baja California: the genera *Rhizosolenia*, *Proboscia*, *Pseudosolenia*, and former *Rhizosolenia* species. *Diatom Research, 10*(2), pp. 251–267.

Jansen, J.H.F., Kuijpers, A. and Troelstra, S.R., 1986. A mid-Brunhes climatic event: Long-term changes in global atmosphere and ocean circulation. *Science, 232*(4750), pp. 619-622.

Jordan, R.W. and Priddle, J., 1991. Fossil members of the diatom genus *Proboscia*. *Diatom Research, 6*(1), pp. 55–61.

Jordan, R.W. and Ligowski, R., 2004. New observations on Proboscia auxospores and validation of the family Probosciaceae fam. nov. *Vie et Milieu, 54*(2-3), pp. 91-103.

Jousé, A.P., 1961. Miocene and Pliocene marine diatoms from the Far East. *Botanical Material, Spore-Bearing Plants, Botanical Institution, Akad. Nauk SSSR*, *16*, pp.59-70.

Jousé, A.P., 1968. New species of diatoms in bottom sediments of the Pacific and the Sea of Okhotsk. *Nov. Systemat. Plant. Non. Vascular., Acad. Nauk SSSR, 3*, pp. 12-21.

Jousé, A.P., Kozlova, O.G., and Muhina, V.V., 1971. Distribution of diatoms in the surface layer of sediment from the Pacific Ocean. In Funnell, B.M., and Riedel, W.R., Eds., *The micropaleontology of the oceans*. Cambridge University Press. London, UK, pp. 407-422.

Katsuki, K. and Takahashi, K., 2005. Diatoms as paleoenvironmental proxies for seasonal productivity, sea-ice and surface circulation in the Bering Sea during the late Quaternary. *Deep-Sea Research Part II: Topical Studies in Oceanography, 52*(16-18), pp. 2110–2130.

Kemp, A.E., Pike, J., Pearce, R.B. and Lange, C.B., 2000. The “Fall dump”—a new perspective on the role of a “shade flora” in the annual cycle of diatom production and export flux. *Deep Sea Research Part II: Topical Studies in Oceanography*, *47*(9), pp. 2129-2154.

Koç, N., Hodell, D.A., Kleiven, H. and Labeyrie, L., 1999. High-resolution Pleistocene diatom biostratigraphy of Site 983 and correlations with isotope stratigraphy. *1999. Proc. ODP, Sci. Results*, *162*, pp. 51-62.

Koç, N., Labeyrie, L., Manthé, S., Flower, B.P., Hodell, D.A. and Aksu, A., 2001. The last occurrence of Proboscia curvirostris in the North Atlantic marine isotope stages 9-8. *Marine Micropaleontology*, *41*(1), pp. 9-23.

Koç, N. and Flower, B.P., 1998. High-resolution Pleistocene diatom biostratigraphy and paleoceanography of Site 919 from the Irminger Basin. *Proceedings of the Ocean Drilling Program, Scientific Results, 152, 152(3)*, pp. 209–219.

Koç, N. and Scherer, R., 1996. Neogene diatom biostratigraphy of the Iceland Sea site 907. In Thiede, J., Myhre, A.M., Firth, J.V., Johnsson, G.L. and Ruddiman, W.F., editors, *Proceeding of the Ocean Drilling Scientific Results, 151*, pp. 61–74.

Koizumi, I., 1973. The late Cenozoic diatoms of Sites 183–193, Leg 19 Deep Sea Drilling Project. *Creager, JS, Scholl, DW, et al., Init. Repts. DSDP, 19*(30), pp. 805–855.

Koizumi, I., 1975b. Late Cenozoic diatom biostratigraphy in the circum-North Pacific region. *Geol. Soc. Japan J., 81*(10), 611-627.

Koizumi, I and Tanimura, Y., 1985. Neogene latitude biostratigraphy of the middle latitude western North Pacific, Deep Sea Drilling Project Leg 86. Init. Rep. DSDP, 86, pp. 269-300

Koning, E., Van Iperen, J.M., Van Raaphorst, W., Helder, W., Brummer, G.J. and Van Weering, T.C.E., 2001. Selective preservation of upwelling-indicating diatoms in sediments off Somalia, NW Indian Ocean. *Deep Sea Research Part I: Oceanographic Research Papers*, *48*(11), pp. 2473-2495.

Makarova, I.V., 1980, September. Principles of the systematics of *Thalassiosira* Cleve and the significance of its taxonomic characters. *In Proceedings of the 6th International Diatom Symposium. Koenigstein: O. Koeltz*, pp. 1-11.

Mann, D.G., 1999. The species concept in diatoms. *Phycologia, 38*(6), pp. 437–495.

Maslin, M.A., Haug, G.H., Sarnthein, M. and Tiedemann, R., 1996. The progressive intensification of northern hemisphere glaciation as seen from the North Pacific. *Geologische Rundschau*, *85*(3), pp. 452-465.

Medlin, L.K. and Priddle, J. eds., 1990. *Polar marine diatoms*. Cambridge: British Antarctic Survey, pp. 214.

Niebauer, H.J., Bond, N.A., Yakunin, L.P. and Plotnikov, V.V., 1999. Chapter 2: An update on the climatology and sea ice of the Bering Sea*, in Dynamics of the Bering Sea*, Loughlin, T.R., Uni. of Fairbanks, Alaska, pp. 29-60.

Ohtani, K., 1973. Oceanographic structure in the Bering Sea. *Memoirs of the Faculty of Fisheries. Hokkaido University, 21*(1), pp. 65-106.

Onodera, J., Takahashi, K. and Nagatomo, R., 2013. Diatoms, silicoflagellates, and ebridians at Site U1341 on the western slope of Bowers Ridge, IODP Expedition 323. *Deep-Sea Research Part II: Topical Studies in Oceanography*, pp. 1–10.

Round, F.E., Crawford, R.M. and Mann, D.G., (eds.) 1990. *Diatoms: biology and morphology of the genera*. Cambridge University Press. Cambridge, UK, pp. 747.

Sancetta, C., 1982. Distribution of diatom species in surface sediments of the Bering and Okhotsk seas. *Micropaleontology, 28*(3), pp. 221–257.

Sancetta, C. and Silvestri, S., 1984. Diatom stratigraphy of the late Pleistocene (Brunhes) subarctic Pacific. *Marine Micropaleontology, 9*(3), pp. 263–274.

Sancetta, C. and Silvestri, S., 1986. Pliocene-Pleistocene evolution of the North Pacific Ocean-Atmosphere system, interpreted from fossil diatoms. *Paleoceanography*, *1*(2), pp.163-180.

Schrader, H.J., 1973. Cenozoic diatoms from the northeast Pacific, Leg 18. *Init. Rep. DSDP, 18*, pp. 673-797.

Simonsen, R., 1979. The diatom system: ideas on phylogeny. *Bacillaria, 2*, pp. 9-71.

Sims, P. A., Mann, D.G. and Medlin, L.K., 2006. Evolution of the diatoms: insights from fossil, biological and molecular data. *Phycologia, 45*(4), pp. 361–402.

Smith, S.L., 2001. Understanding the Arabian Sea: Reflections on the 1994-1996 Arabian Sea Expedition. *Deep-Sea Research Part II: Topical Studies in Oceanography, 48*(6-7), pp. 1385–1402.

Springer, A.M., McRoy, C.P. and Flint, M.V., 1996. The Bering Sea Green Belt : shelf-edge processes and ecosystem production. *Fisheries Oceanography*, *5*(3-4), pp. 205-223.

Stabeno, P., Schumacher, J.D. and Ohtani, K., 1999. The physical oceanography of the Bering Sea. *Dynamics of the Bering Sea,* pp. 1–60.

Stroynowski, Z., Ravelo, A.C. and Andreasen, D., 2015. A Pliocene to recent history of the Bering Sea at Site U1340A, IODP Expedition 323. *Paleoceanography*, pp. 1–16.

Sukhanova, I.N., Flint, M.V., Whitledge, T.E., Stockwell, D.A. and Rho, T.K., 2006. Mass development of the planktonic diatom Proboscia alata over the Bering Sea shelf in the summer season. *Oceanology*, *46*(2), pp. 200-216.

Sunesen, I.N. and Sar, E.A., 2007. Marine diatoms from Buenos Aires coastal waters (Argentina). IV. Rhizosolenia s. str., Neocalyptrella, Pseudosolenia, Proboscia. *Phycologia, 46*(6), pp. 628–643.

Sundström, B.G., 1986. The marine diatom genus Rhizosolenia: a new approach to the taxonomy. PhD thesis. Lund University. pp. 117.

Suto, I., 2004. Taxonomy of the diatom resting spore form genus *Liradiscus* Greville and its stratigraphic significance. *Micropaleontology, 50*(1), pp. 59–79.

Syvertsen, E.E., 1985. Resting spore formation in the antarctic diatoms *Coscinodiscus furcatus* Karsten and *Thalassiosira australis* Peragallo. *Polar Biology, 4*(2), pp.113–119.

Takahashi, K., 2005. The Bering Sea and paleoceanography. *Deep-Sea Research Part II: Topical Studies in Oceanography, 52*(16-18), pp. 2080–2091.

Takahashi, K., Jordan, R. and Priddle, J., 1994. The diatom genus *Proboscia* in Subarctic Waters. *Diatom Research, 9*(2), pp. 411–428.

Takahashi, K., Ravelo, A.C. and Zarikian, C.A., 2011a. IODP Expedition 323-pliocene and pleistocene paleoceanographic changes in the Bering Sea. *Scientific Drilling, 11*, pp. 4–13.

Takahashi, K., A. C. Ravelo, C. Alvarez Zarikian, and the IODP Expedition 323 Scientists, 2011b. Proc. IODP 323. *Integrated Ocean Drilling Program Management International, Tokyo*, pp. 1-81.

Teraishi, A., Suto, I., Onodera, J. and Takahashi, K., 2013. Diatom, silicoflagellate and ebridian biostratigraphy and paleoceanography in IODP 323 Hole U1343E at the Bering slope site. *Deep Sea Research Part II: Topical Studies in Oceanography*, pp. 1-11.

Tréguer, P.J. and De La Rocha, C.L., 2013. The world ocean silica cycle. *Annual review of marine science, 5*(1), pp. 477–501.

Treppke, U.F., Lange, C.B., Donner, B., Fischer, G., Ruhland, G. and Wefer, G., 1996. Diatom and silicoflagellate fluxes at the Walvis Ridge: an environment influenced by coastal upwelling in the Benguela system. *Journal of Marine Research, 54*(5), pp. 991-1016.

Tsukazaki, C., Ishii, K.I., Saito, R., Matsuno, K., Yamaguchi, A. and Imai, I., 2013. Distribution of viable diatom resting stage cells in bottom sediments of the eastern Bering Sea shelf. *Deep-Sea Research Part II: Topical Studies in Oceanography, 94*, pp. 22–30.

Villareal, T.A., 1988. Positive buoyancy in the oceanic diatom *Rhizosolenia debyana* H. Peragallo. *Deep Sea Research Part A, Oceanographic Research Papers, 35(*6), pp. 1037–1045.

Von Quillfeldt, C.H., 2000. Common diatom species in Arctic spring blooms: Their distribution and abundance. *Botanica Marina, 43*(6), pp. 499–516.

Von Quillfeldt, C.H., 2001. Identification of some easily confused common diatom species in arctic spring blooms. *Botanica Marina, 44*(4), pp. 375–389.

Von Quillfeldt, C.H., Ambrose Jr, W.G. and Clough, L.M., 2003. High number of diatom species in first-year ice from the Chukchi Sea. *Polar Biology, 26*(12), pp. 806-818.

Yanagisawa, Y. and Akiba, F., 1998. Refined Neogene diatom biostratigraphy for the Northwest Pacific around Japan, with an introduction of code numbers for selected diatom biohorizons. *Jour. Geol. Soc. Japan, 24*(6), pp. 395-414.

8 Plates

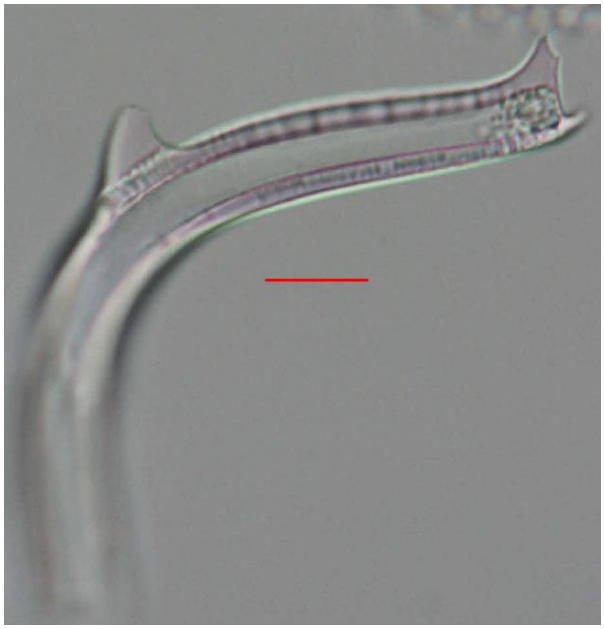

1

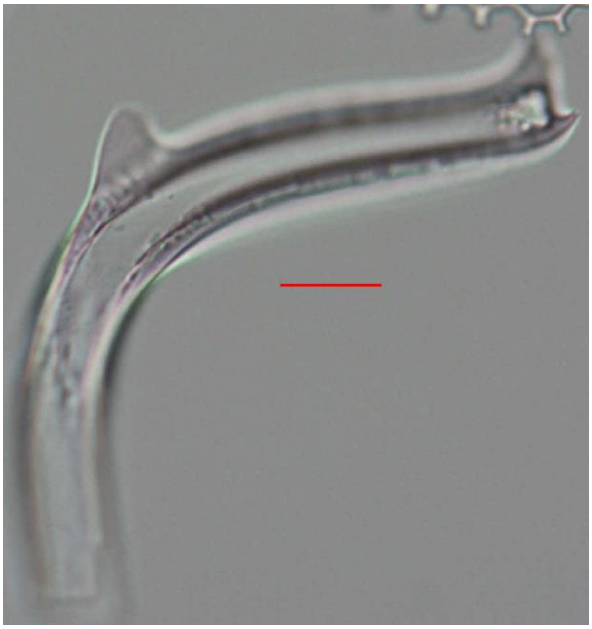

2

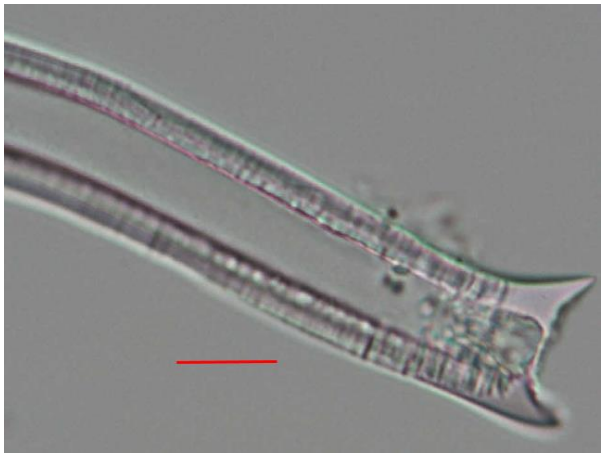

3

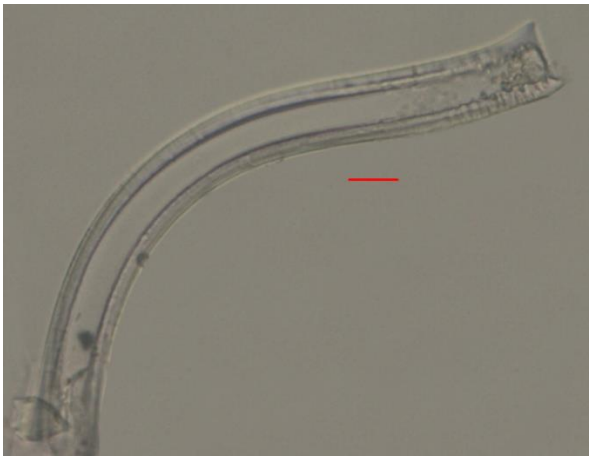

4

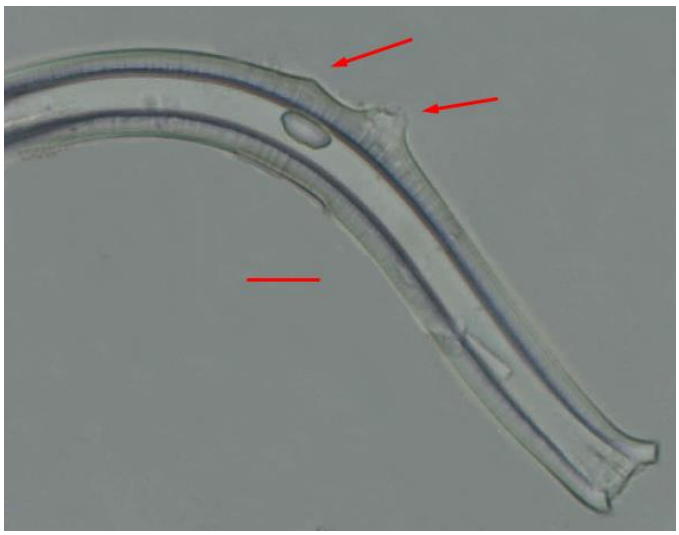

5

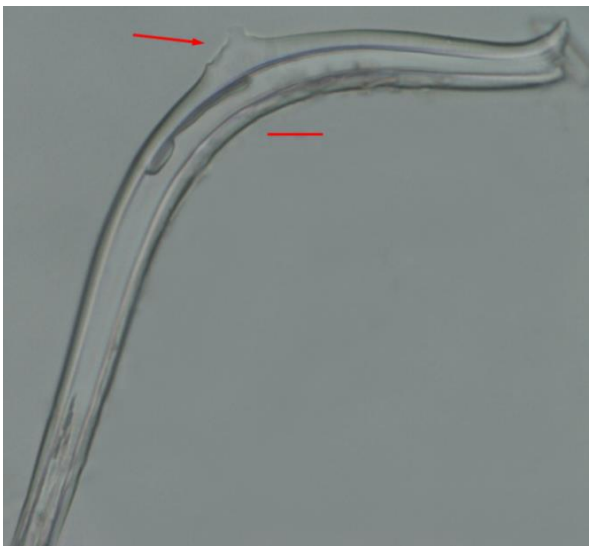

6

Plate 1 - Scale bar = 10 µm. All figures are light microscope (LM) images at 1000x or 600x magnifications. 1, 2 – *Proboscia curvirostris* (same specimen; 1000x; sample U1340A-14H3, 121.95 m); 3 – *Proboscia barboi* (distal end; 1000x; sample U1340A-11H-CC, 99.17 m); 4 – *P. barboi* (600x; sample U1340A-11H-CC, 99.17 m); 5, 6 – Intermediate specimens (600x; sample U1340A-24H-5, 203.54 m). Arrows denote incipient “dorsal fins”.

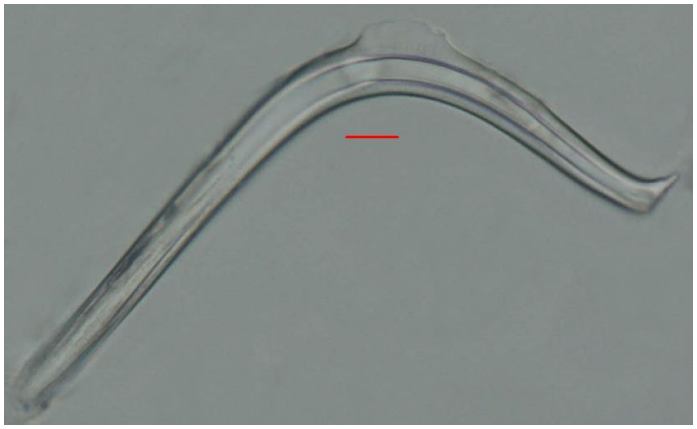

1

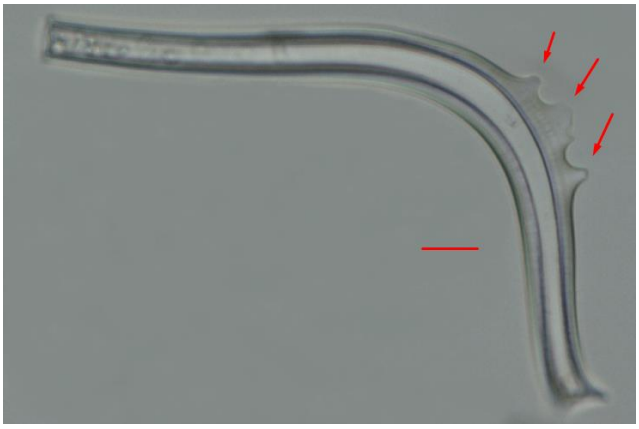

2

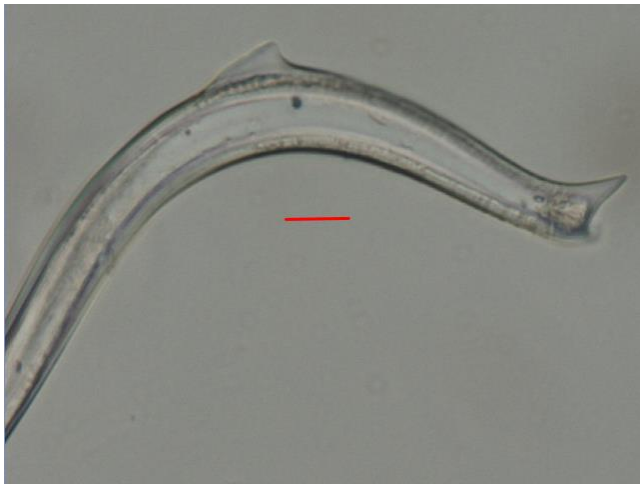

3

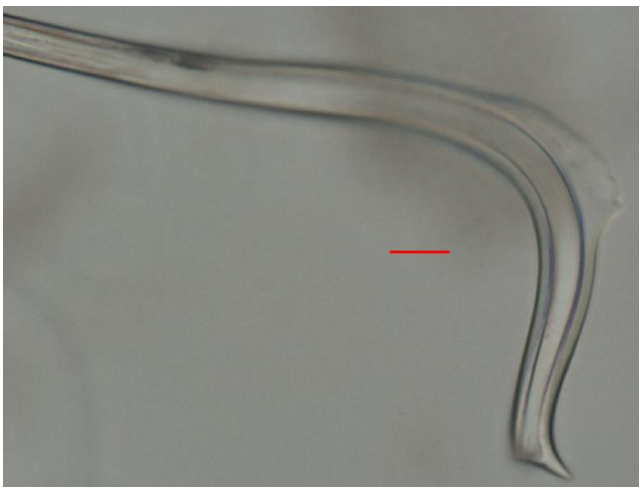

4

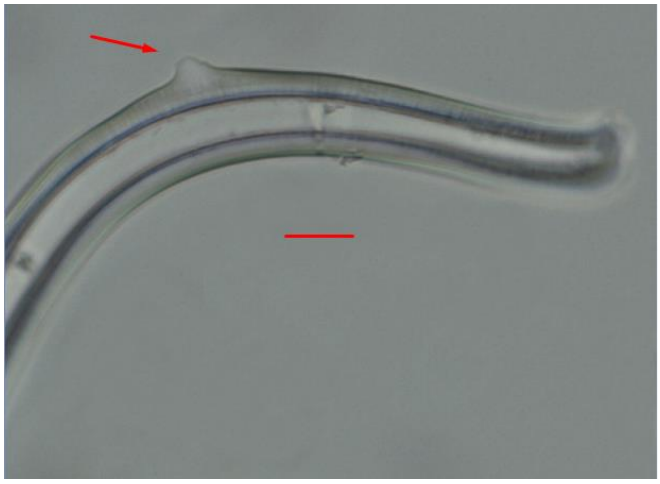

5

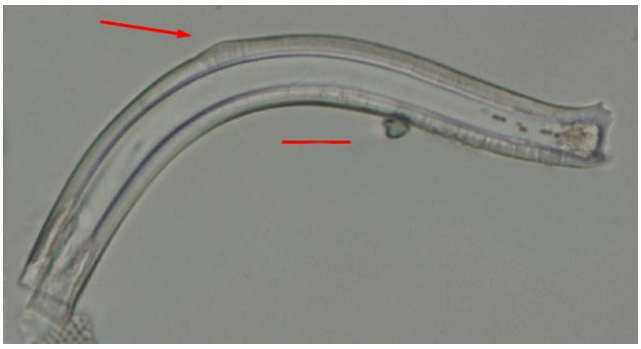

6

Plate 2 - Scale bar = 10 µm. All figures are LM images of intermediate specimens at 600x magnification (sample U1340A-24H5, 203.54 m). Arrows denote incipient “dorsal fins”.

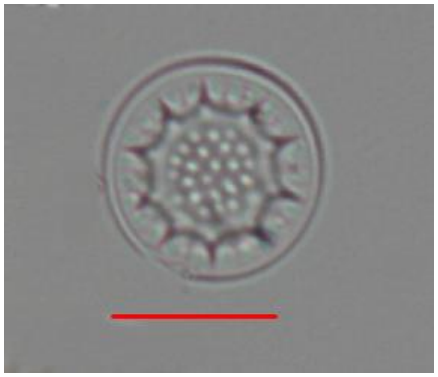

1

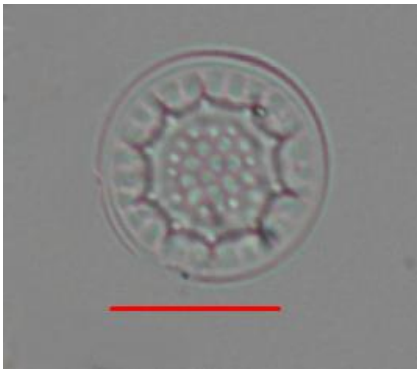

2

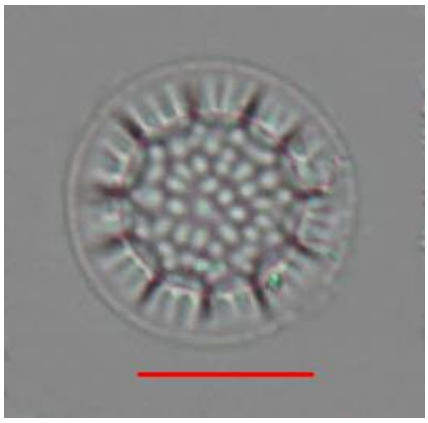

3

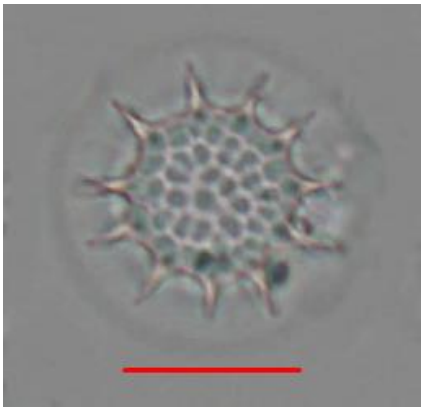

4

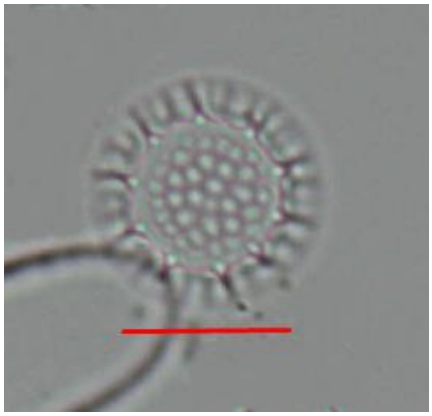

5

6

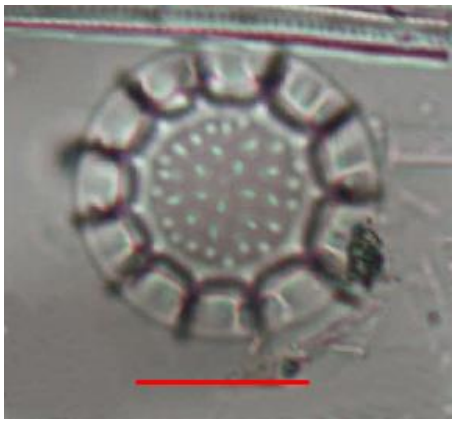

7

8

Plate 3 – Scale bar = 10 µm. All figures are LM images of *Thalassiosira jouseae* at 1000x magnification. 1, 2 – Sample U1340A-10H-CC, 89.63 m (same specimen); 3, 4 – Sample U1340A-7H-CC, 61.20 m (same specimen); 5, 6 – Sample U1340A-10H-3, 84.26 m (same specimen); 7, 8 – sample U1340A-15H5, 134.89 m (same specimen).

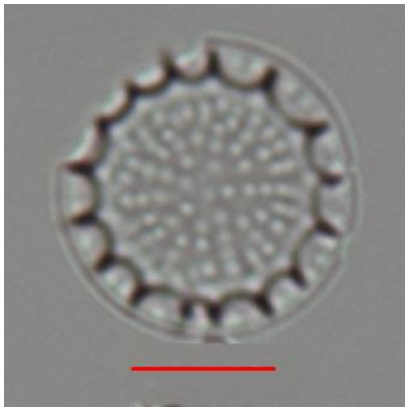

1

2

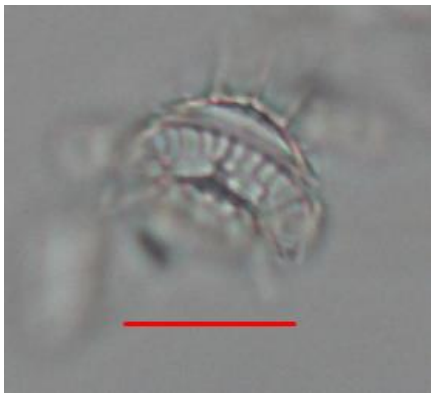

3

4

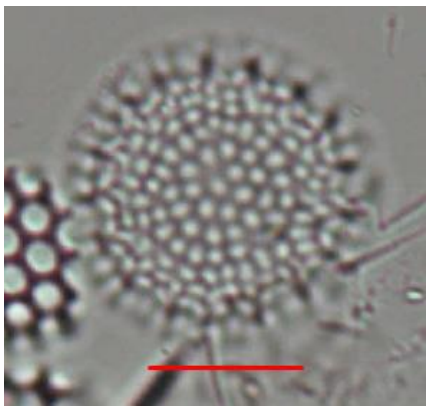

5

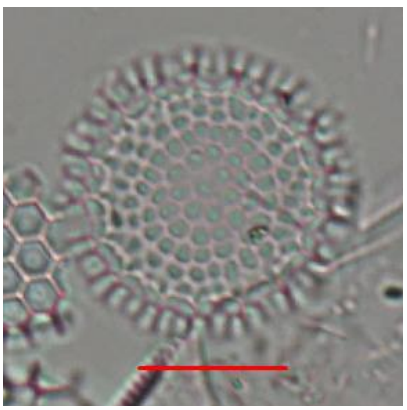

6

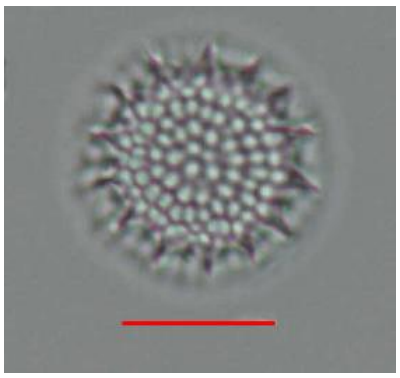

7

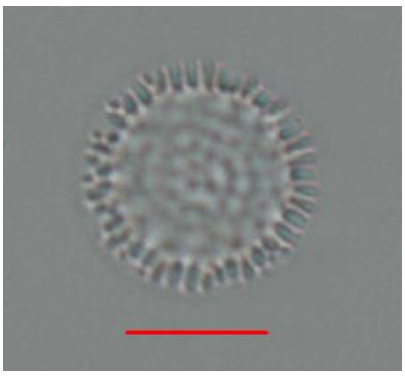

8

Plate 4 - Scale bar = 10 µm. All figures are LM images of *Thalassiosira jouseae* (except for 7 and 8) at 1000x magnification. 1 – Sample U1340A-14H6, 126.75 m; 2, 3, 4 – Sample U1340A-10H-CC, 89.63 m (girdle view; 3 and 4 same specimen); 5, 6 - Sample U1340A-15H5, 134.89 m (same specimen); 7, 8 – *Thalassiosira nidulus*, Sample U1340A-9H-3, 75.95 m (same specimen).

Annex

9 Diatom study of the Miocene of the Lower Tagus Basin

Introduction

The study of Portuguese diatoms began in the late XIX century, most works consisting of identification and cataloguing of living specimens. Perhaps the most prolific naturalist in this field was Carlos Zimmermann who catalogued and compiled hundreds of diatom species from 1906 to 1910. Concerning fossil diatoms few systematic studies were made, being noteworthy to mention "Diatomáceas Fósseis de Portugal - Jazigos de Rio-Maior, Óbidos e Alpiarça" of Alfredo da Silva (1946), which consists in a literature review of previous works and a contribution to the discovery of diatom taxa of Portugal. This present study covers the diatoms of the Belverde Borehole and a couple of samples from the Penedo Norte outcrop, which have not yet been studied in this borehole.

The Cenozoic of the Lower Tagus Basin

The Lower Tagus Basin is a Cenozoic basin that occupies a large area of approximately 260 Km long and 80 Km wide) in central south Portugal, extending SW-NE from the coastal region of Lisboa-Setúbal, beyond the border with Spain near Castelo Branco (Pais et al., 2012). Since at least the XVIII century, it has been object of various geologic and paleontologic studies and presents a fairly complete Neogene sedimentary record that includes marine and continental facies and a diverse and abundant paleontologic content. The LTB is furthermore characterized by its privileged geographic position allowing comparison between the Atlantic and Mediterranean domains. Thus, the LTB stands as a good reference to other European Cenozoic basins regarding Stratigraphy, Paleontology and other geologic fields.

The LTB can be divided in three main sectors:

- the distal sector, in the regions of Setubal Peninsula and Lisboa;
- the intermediate sector, occupying a broad area in Ribatejo and part of Alto Alentejo;
- the proximal sector, in Southern Beira Baixa, crossing the border with Spain.

Throughout all the Neogene Era, the LTB suffered tectonic phenomena and underwent several cyclic marine transgressions and regressions, which resulted in geographic changes and shifts between continental and marine sedimentary systems, mainly in the distal sector, but also affecting the intermediate sector. The basal infill of the LTB dates back to Middle Eocene and is comprised of poorly sorted alluvial materials, originating from the nearby Hesperian Massif, often accumulated through alluvial fans. During the Paleogene, sedimentation in the LTB basin is solely endorheic (i.e. continental) and lithologies are characterized by coarse conglomeratic materials interbedded with sandstone layers and occasionally lacustrine or marsh limestones. In Lisboa-Setubal Peninsula these deposits constitute the Benfica formation.

The first marine transgression only took place in the Aquitanian, about 24 Ma, when the Atlantic invaded the distal sector from the South, thereby forming a narrow and penetrative gulf. A high sea bed oriented N-S, approximately coincident with the existing shoreline protected the inner sector of the gulf and likely favored the establishment of a coralline barrier from at least Belverde to Lisboa. Thereafter, sedimentation in the LTB occurred at the continent-ocean interface; The areas of the basin farther from the coast receiving more materials from the fluvial system (i.e. Pre-Tejo River) running from NE to SW and coastal marine sedimentation in the distal sector and to some extent the intermediate sector. The shoreline and geographic extent of the gulf suffered considerable oscillations according to the eustatic cycles. The most expressive transgressions occurred in middle Burdigalian (~18 Mya), late Langhian (~ 14 Mya) and early Tortonian (~ 11 Mya). During the middle Burdigalian and late Langhian transgressions,

the waters advanced circa 100 km into the basin and reached the vicinities of Santarem in the intermediate sector (Pais et al., 2012).

Geologic setting of the distal sector

The Miocene deposits of the distal sector form a sucession from the Aquitanian to the Tortonian and are integrated in the Albufeira Syncline, which encompasses the area from the Arrábida Chain to North Lisbon (fig. 1). In terms of thickness, the Miocene sucession does not exceed 300 m in Lisboa, while in the Barreiro and Montijo regions (Setúbal), the Neogene reaches 1200 m, 50 m belonging to the Pliocene. This Miocene sucession is separated from the underlying deposits (Lower Cretaceous, the Vulcanic Complex of Lisboa-Mafra or the Benfica Formation) by an angular unconformity and is strongly eroded by the Pliocene (Legoinha, 2001).

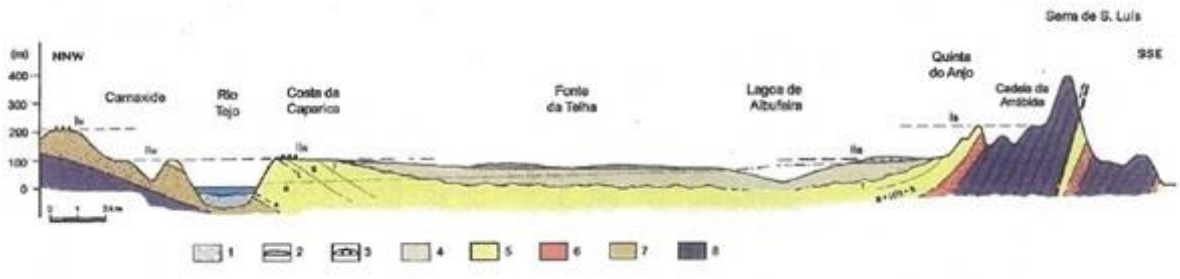

Figure 1 – Geologic profile of the Setubal Peninsula. 1- alluvia (Holocene); 2- aeolic dunes (Holocene); 3- Formação de Marco Furado (Plio-Quaternary); 4- Pliocene; 5- Miocene (A- Aquitanian, B- Burdigalian, L- Langhian, S- Serravalian, T- Tortonian); 6- Paleogene; 7- Vulcanic complex of Lisboa (Upper Cretaceous); 8- Mesozoic. (Legoinha, 2001).

Paleoenvironmental remarks

Since the Aquitanian, tropical conditions and warm waters were predominant in marine areas as evidenced by fossil remains of corals. Maximum temperatures comparable to the present day Gulf of Guinea were reached in the late Burdigalian and Langhian rapidly decreasing to temperatures similar to those of the present day Moroccan coast. Fauna and vegetation assemblages indicate alternating episodes of aridity and humidity, the dryest one during the Langhian (Antunes and Pais, 1984; Antunes, 1993; Pais, 2012).

Water depth oscillated frequently throughout the Miocene, having marine environments shifted from littoral (i.e. intertidal) to infra-littoral depths and attaining a circa-littoral depth during the Serravalian. Paleobathymetry studies employing benthic foraminifera of samples from the Penedo Norte section indicate a circa-litoral environment during Late Burdigalian (145 m +/- 40), a rise in water depth in Laghian-Serravalian (170 m +/- 45) and a shallower depth in Early Tortonian (65 m +/- 15; Legoinha and Corbi, 2012)

Sondagem de Belverde

The Belverde drilling project started in 2001 by a research team from Centro de Estudos Geológicos (UNL) coordinated by M. T. Antunes and aimed to obtain the most continuous record of the Neogene deposits of Setúbal Peninsula (distal sector of LTB) in order to perform stratigraphic studies and uncover the past environmental and geographic conditions of the region (Pais et al., 2003; Legoinha et al., 2004). Location: Península de Setúbal, coordinates: 38° 35' 54, 1'' N; 9° 8' 24, 7'' W).

The borehole attained 619, 77 m depth crossing 130 of Plio-Pleistocene continental deposits, 460 m of Miocene deposits (from 130-590 m), and also reached the topmost Paleogene

deposits (fig. 2). The main Miocene lithologies are fine sands, marls and biocalcarenites. Coral reefs were recognized in the Aquitanian, Burdigalian and Langhian (Legoinha et al., 2004).

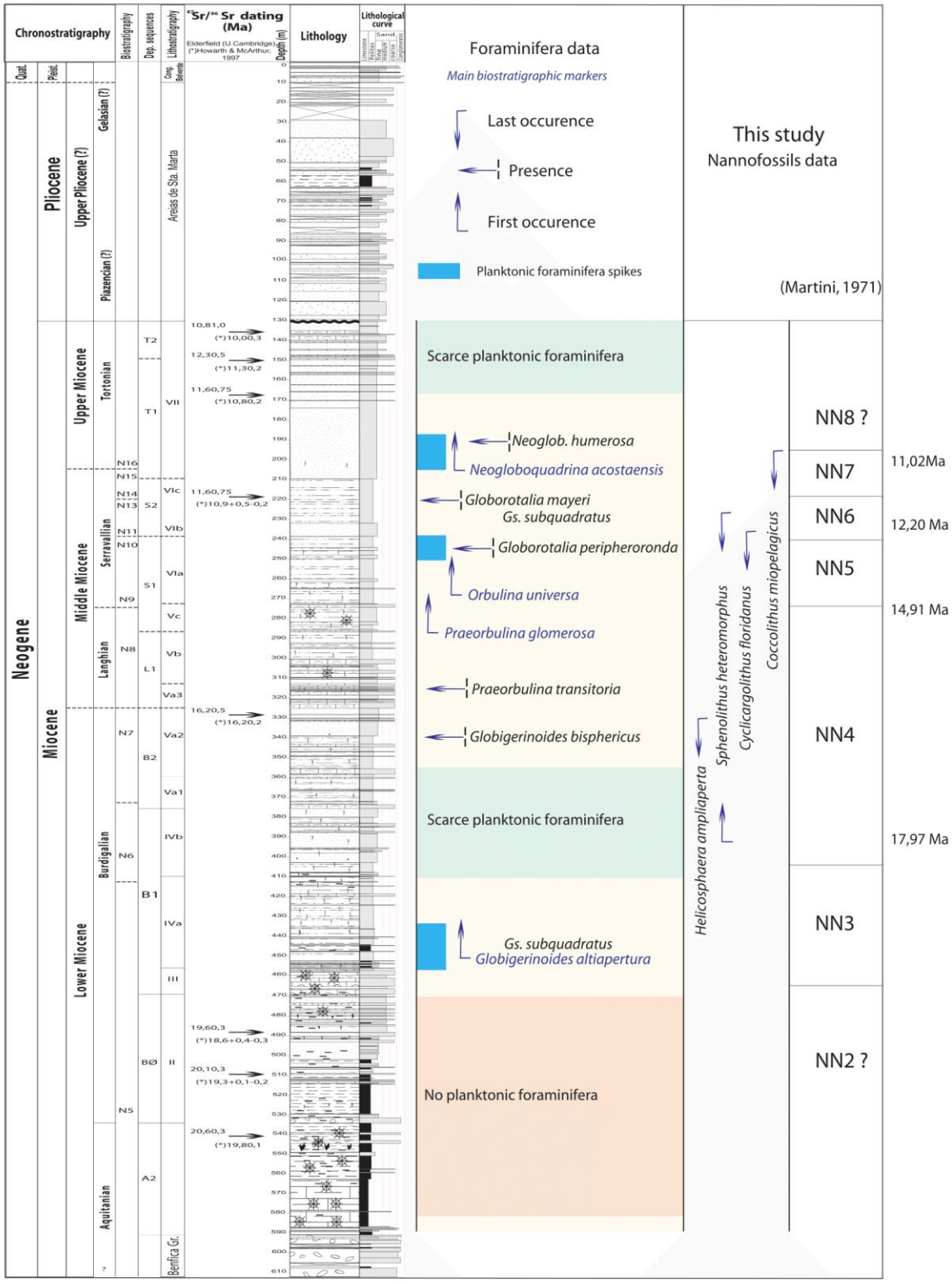

Figure 2 – Sedimentary sequence of the Belverde core displaying the $^{87}Sr/^{86}Sr$ ages and biostratigraphy of foraminifera and nanofossils (Legoinha and Flores, 2014).

Penedo Norte section

This outcrop consists of the North cliff of Penedo beach in Sesimbra, Setubal Peninsula. Military coordinates (folha 464-Sesimbra, Carta Militar de Portugal, 1:25 000, Serviços Cartográficos do Exército) of the sampling location: M – 107.650 Km and P – 167.200 Km; Coordinates GPS: 38º 27' 46'' N; 9º 11' 31'' W. (Legoinha, 2001)

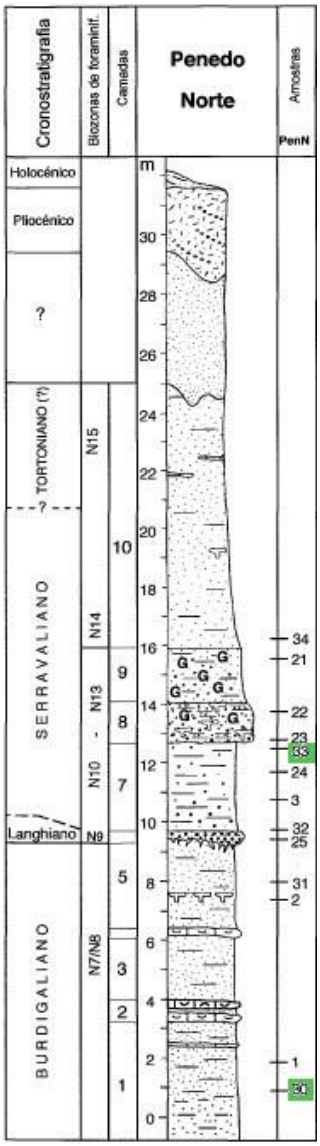

Figure 3 – Penedo Norte section. Samples studied highlighted in green. Adapted from Legoinha (2001).

The Penedo Norte section (fig. 3) spans from Burdigalian to Holocene and is divided in three sequences separated by disconformities: B2 (Upper Burdigalian), S1 (Langhian-Serravalian) and T1 (Lower Tortonian). The Samples PN30 and PN33 were recovered from layer 1 (grey micaceous clayey silts) and 7 (grey sandstone) and roughly correspond to 350-360 m and 243 m deep in the Belverde core, respectively.

Methods

This study is based on 41 samples of sediment from the Belverde drill core plus 2 samples (PN30 and PN33) taken from the Penedo Norte outcrop (Table 1). Sampling was performed by selecting sediments from all across the core's Miocene record, giving preference to darker facies, which are indicative of higher organic content. The core samples range from 141 m (Upper Miocene) to 557 m (Lower Miocene) in depth. The outcrop samples were collected from the North Cliff of the Penedo beach, Setubal Peninsula (GPS coordinates: 38° 27' 46" N; 9° 11' 31" W; Legoinha, 2001).

In order to attain an overview of the diatom content of the samples, a total of 51 smear slides were prepared. Preliminary observations indicated that none to very little diatomaceous content is present on the smear slides. Taking this into account, the bulk sediment used in the cleaning treatments was doubled to 2 g, instead of the standard 1 g, to increase the likelihood of finding diatoms on the slides.

The sample cleaning method used is derived from Barron's procedure for rapid sample preparation at sea (Barron, 1985), adapted and modified by Abrantes et al. (2005). This treatment eliminates all clay minerals, carbonates and organic matter from the sediments so that the siliceous material is concentrated and more easily observed on the final slides.

Cleaning procedure

Approximately 2 g of bulk sediment was weighed and treated in 250 ml cups with the following solutions:

- 25 ml 0.33% calgon water softener to disperse the clays and disaggregate the sediment.
- 25 ml 10% HCl to destroy the carbonates.
- Add 25 ml 30% H2O2 to destroy organic matter.

Afterwards, samples went through the washing process, which removes the clay minerals in suspension and leaves behind the siliceous material as the former takes much less time to settle. The material was filled to the 250 ml mark. After an 8 hour settling period, the clay in suspension was removed using vacuum pump suction. This procedure was repeated for approximately two weeks until solutions had a clear and transparent appearance, free from clays.

Slide preparation

Slide preparation was performed following the Battarbee's method (1973) in which a known volume of homogenized solution (i.e. aliquot; Table 1) was poured into circular trays previously set with 4 cover slips and covered in water. Subsequently, the trays were left to rest in an undisturbed environment so the particles in suspension could randomly settle on the cover slips. After the trays were completely dry, cover slips were mounted on slides using Norland Optical Adhesive.

Microscope observations

All samples were thoroughly scanned for siliceous microfossils at 1000x magnification. Microscope used: Nikon eclipse 80i.

Table 1 – Samples (Belverde Borehole and Penedo Norte, correspondent core depth, weight of treated sediment, and aliquot poured into the circular tray. Depth values were rounded to the first decimal place.

Samples	Core depth (m)	Weight (g)	Aliquot (ml)
1	141.5	2.0601	3
2	142.4	2.6569	4
3	154.0	2.3006	3
4	170.8	2.2857	5
5	179.7	2.3346	7
6	193.8	2.1796	6
7	213.5	2.2891	8
8	214.0	2.1791	10
9	217.0	2.6439	10
10	218.6	2.1370	4
11	219.3	2.5437	5
12	230.3	2.3777	6
13	239.0	2.2277	4
14	239.8	2.7299	9
15	241.3	2.4882	9
16	243.5	2.6218	4
17	252.3	2.2853	5
18	255.9	2.6815	6
19	259.6	6.8552	4
20	273.5	2.6523	6
21	305.0	2.1004	3
22	336.1	2.5839	3
23	338.7	2.6523	3
24	352.4	2.6447	4
25	353.4	2.4931	2
26	379.8	2.2849	3
27	382.6	2.4626	3
28	384.7	2.4833	3
29	390.9	2.5663	8
30	404.8	2.3123	2
31	412.2	2.2484	2
32	445.3	2.4516	1
33	448.4	2.2481	3
34	455.1	2.4160	1
35	491.2	2.4513	2
36	503.8	2.2188	3
37	515.8	2.1471	1
38	521.7	2.6542	5
39	522.3	2.2795	4
40	529.0	2.5075	4
41	557.9	2.6428	9
PN30	-	2.4826	3
PN33	-	2.5492	2

Results

No microfossils whatsoever were found in any of the samples, except for sample PN33 in which small raphid pennate diatoms occur, although very rarely. A few other structures were found such as hexagonal-shaped structures. The following genera were identified:

Mastogloia sp.

Mastogloia is a large genus of epipelic and epiphytic diatoms found in marine and freshwater environments. The diagnostic feature of this genus is the row of chambers (partecta) usually running longitudinally along the interior valve wall. Only one specimen of this genus was found (fig. 4) and the position of the partecta, being apparently dislocated towards the centre of the valve, indicates that this specimen belongs to group Paradoxae (*sensu* Hustedt, 1985) of *Mastogloia*.

Figure 4 – *Mastogloia sp.* in valve view. Scale bar = 10 µm.

Epithemia sp.

Epithemia is an exclusively freshwater genus of epiphytic and epipelic diatoms. Only one frustule belonging to this genus can be assuredly identified. In the right-hand valve of the specimen, it can be observed the V-shaped raphe which is diagnostic of the genus (fig. 5). In other similar frustules, 2 of them found in association with the *Epithemia* frustule, the V-shaped raphe is either not visible or lacking. In the latter case, these frustules most likely belong to *Rhopalodia* sp.

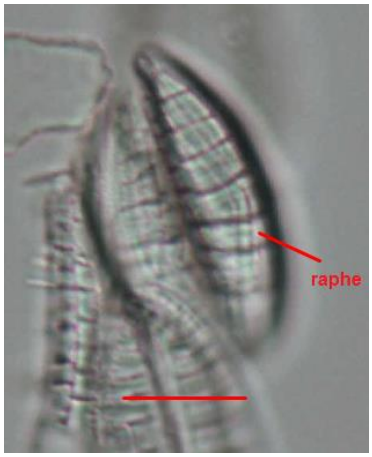

Figure 5 – Frustules of *Epithemia* sp. with the V-shaped raphe. Scale bar = 10 µm.

***Rhopalodia* sp.**

Rhopalodia is a genus of epipelic and epiphytic diatom of fresh and marine waters. In this genus, the raphe runs along the dorsal margins of the valves. In some specimens it is possible to distinguish a striated pattern along the dorsal margin which probably corresponds to the raphe. Some specimens also display a small notch in the middle of the dorsal margin of the valves, a feature often observed in *Rhopalodia* species (fig. 6). Several frustules belonging to either *Epithemia* or *Rhopalodia* were recurrent but no exact identification was possible.

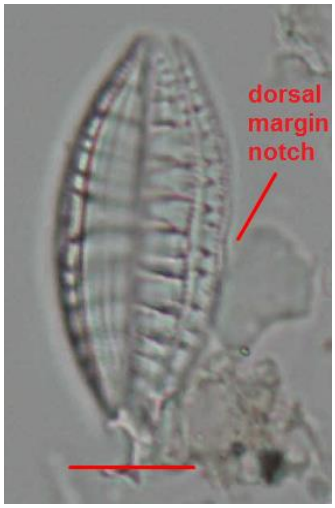

Figure 6 – Frustules of *Rhopalodia sp.* Scale bar = 10 µm.

***Amphora* sp.**

Amphora is a genus of pennate diatoms, mainly of marine waters, with some freshwater species. The frustule is wedge-shaped like an orange segment and is usually observed in girdle view. The only specimen found can be observed along the narrow edge of the frustule, which is a rather unusual view (fig. 7).

Figure 7 – *Amphora* sp. (girdle view). Scale bar = 10 µm.

Naviculoid valve fragment

One valve fragment belonging to genus *Navicula* or a related genus was found (fig. 8). Navicula is a genus of marine and freshwater epipelic diatoms.

Figure 8 – Valve fragment of a naviculoid diatom. Scale bar = 10 µm

Raphid pennate diatoms

Some frustules could not be identified further than raphid pennate diatoms (fig. 9 and 10; different species). Only one specimen like the one of figure 9 was found. Specimens similar to figure 10 were somewhat recurrent.

Figure 9 – Raphid pennate diatom (girdle view). Scale bar = 10 µm

Figure 10 – Rhaphid pennate diatom (girdle view). Scale bar = 10 µm

Hexagonal structures

Hexagonal structures (fig. 11, 12, 13 and 14), with 10 µm or less, morphologically variable, were as recurrent as diatoms. The nature of these structures is uncertain although they are not diatom valves nor derive from diatom structures. Pollen grains can also be excluded as they have a larger size. Possibly, they are some kind of phytoliths of higher plants (siliceous structures found in plant tissues), although phytoliths do not have such well-defined hexagonal outlines as the specimens found. Therefore, the identification of these structures remains open.

Figure 11 – Hexagonal structure. Seems organic and contains a circular body in the interior. Scale bar = 10 µm.

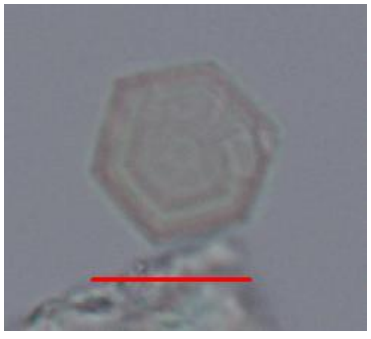

Figure 12 – Hexagonal structure. Interior seems to contain another hexagonal outline. Scale bar = 10 µm.

Figure 13 – Hexagonal structure. At least two faint lines crossing from the edge to the centre. Scale bar = 10 µm.

Figure 14 – Three adjacent hexagonal structures. Scale bar = 10 µm.

Discussion

The absence of microfossils in the drill core samples can be attributed to low sedimentation rates and poor preservation during and after deposition in the sediments of the LTB. Only sample PN33, from the Penedo Norte outcrop, contained diatoms and other siliceous structures. For a number of reasons the diatoms found are likely a result of *in situ* contamination. One strong reason, is the presence of at least one *Epithemia* frustule, an exclusively freshwater genus, which is highly unlikely in a marine deposit during the Serravalian transgression. Furthermore, only pennate benthic specimens were present in the sample, whereas no planktonic species were found, which does not represent a marine diatom assemblage. Lastly, the presence of complete frustules (with both valves and connecting girdle bands) is unlikely in material as old as Miocene material.

Conclusions

- The Belverde borehole is barren of siliceous microfossils.
- Only sample PN33, from the Penedo Norte outcrop yielded benthic raphid pennate diatoms and some unidentified hexagonal structures.
- The diatoms found in sample PN33 are most likely a result of *in situ* contamination as they not represent well a marine diatom assemblage and also due to the presence of *Epithemia* sp. (a fresh water genus).
- Identified genera: *Mastogloia* sp., *Epithemia* sp., *Rhopalodia* sp., *Amphora* sp.

References

Abrantes, F., Gil, I., Lopes, C. and Castro, M., 2005. Quantitative diatom analyses—a faster cleaning procedure. *Deep Sea Research Part I: Oceanographic Research Papers*, *52*(1), pp. 189-198.

Andrade da Silva A., 1946. Diatomáceas fósseis de Portugal - Jazigos de Rio Maior, Óbidos e Alpiarça. *Boletim da Sociedade Geológica de Portugal, VI* (I e II), pp. 5-166.

Antunes M.T. and Pais J., 1984. Climate during Miocene in Portugal and its evolution. *Paléobiol. Continent 14*(2): 75–89.

Antunes, M.T. and Pais, J., 1993. The Neogene of Portugal. *Ciências da Terra 12*, pp. 7–22.

Barron, J., 1985. Late Eocene to Holocene diatom biostratigraphy of the equatorial Pacific Ocean, Deep Sea Drilling Project Leg 85. *Initial Reports of the Deep Sea Drilling Project. US Government Printing Office, Washington, 85* (OCT), pp. 413–456.

Battarbee, R., 1973. A new method for estimating absolute microfossil numbers with special reference to diatoms. *Limnology and Oceanography, 18*, 647–653.

Hustedt, F., 1985. The Pennate Diatoms. Koeltz Scientific Books, Hirschberg, Germany.

Legoinha, P., Sousa, L., Pais, J., Ferreira, J., Amado, A.R. and Ribeiro, I., 2004. Miocene lithological, foraminiferal and palynological data from the Belverde borehole (Portugal). *Revista Española de Paleontología, 11*(2), pp. 243-250.

Legoinha, P. and Corbi, H., 2012. Benthic foraminifera and palaeodepth assessment of the Late Burdigalian, Langhian Serravallian and Early Tortonian transgressions in the Lower Tagus Basin, Portugal. *Libro de Resúmenes*, pp. 79-81.

Legoinha, P. and Flores, A. J., 2014. Refinement of the biostratigraphy and biochronology of the Belverde borehole (Setúbal Peninsula, Portugal) using calcareous nannofossil data. *R. Rocha et al. (eds), STRATI 2013, Springer Geology*, pp. 1119-1122.

Pais, J., Cunha, P.P., Pereira, D., Legoinha, P., Dias, R., Moura, D., da Silveira, A.B., Kullberg, J.C. and González-Delgado, J.A., 2012. *The Paleogene and Neogene of Western Iberia (Portugal): A Cenozoic Record in the European Atlantic Domain*. Springer. Berlin, Heidelberg, pp. 138.

Pais J., Silva Lopes, C., Legoinha, P., Ramalho, E., Ferreira, J., Ribeiro, I., Amado, A. R., Sousa, L., Torres, L., Baptista, R. and Reis, R. P., 2003 – Sondagem de Belverde (Bacia do Baixo Tejo, península de Setúbal, Portugal). VI Cong Nacional Geologia, *Ciências da Terra (UNL)*, nº esp. V: 13, CDRom A99-A102.